



A 15-year record of CO emissions constrained by MOPITT CO observations

Zhe Jiang^{1,2}, John R. Worden¹, Helen Worden², Merritt Deeter², Dylan B. A. Jones³, Avelino F. Arellano⁴, and Daven K. Henze⁵

¹Jet Propulsion Laboratory, California Institute of Technology, Pasadena, CA, USA

²Atmospheric Chemistry Observations and Modeling Laboratory, National Center for Atmospheric Research, Boulder, CO, USA

³Department of Physics, University of Toronto, Toronto, ON, Canada

⁴Department of Hydrology and Atmospheric Sciences, University of Arizona, Tucson, AZ, USA

⁵Department of Mechanical Engineering, University of Colorado, Boulder, CO, USA

Correspondence to: Zhe Jiang (zhejiang@ucar.edu)

Received: 11 September 2016 – Discussion started: 17 October 2016

Revised: 11 March 2017 – Accepted: 19 March 2017 – Published: 6 April 2017

Abstract. Long-term measurements from satellites and surface stations have demonstrated a decreasing trend of tropospheric carbon monoxide (CO) in the Northern Hemisphere over the past decade. Likely explanations for this decrease include changes in anthropogenic, fires, and/or biogenic emissions or changes in the primary chemical sink hydroxyl radical (OH). Using remotely sensed CO measurements from the Measurement of Pollution in the Troposphere (MOPITT) satellite instrument, in situ methyl chloroform (MCF) measurements from the World Data Centre for Greenhouse Gases (WDCGG) and the adjoint of the GEOS-Chem model, we estimate the change in global CO emissions from 2001 to 2015. We show that the loss rate of MCF varied by 0.2 % in the past 15 years, indicating that changes in global OH distributions do not explain the recent decrease in CO. Our two-step inversion approach for estimating CO emissions is intended to mitigate the effect of bias errors in the MOPITT data as well as model errors in transport and chemistry, which are the primary factors contributing to the uncertainties when quantifying CO emissions using these remotely sensed data. Our results confirm that the decreasing trend of tropospheric CO in the Northern Hemisphere is due to decreasing CO emissions from anthropogenic and biomass burning sources. In particular, we find decreasing CO emissions from the United States and China in the past 15 years, and unchanged anthropogenic CO emissions from Europe since 2008. We find decreasing trends of biomass burning CO emissions from boreal North

America, boreal Asia and South America, but little change over Africa. In contrast to prior results, we find that a positive trend in CO emissions is likely for India and southeast Asia.

1 Introduction

Tropospheric CO is a product of incomplete combustion and a byproduct of the oxidation of hydrocarbons. It plays a key role in atmospheric chemistry because it is the main sink for OH and an important precursor for tropospheric ozone (O₃). Recent studies have demonstrated significant change in tropospheric CO abundance in the past decade. Using Atmospheric Infrared Sounder (AIRS) CO measurements, Warner et al. (2013) indicated that the Northern Hemispheric CO mixing ratio decreased by 1.28 ppb yr⁻¹ in the period of 2003–2012. Worden et al. (2013a) demonstrated that Northern Hemispheric CO column measurements from MOPITT show a decrease of ~0.92 % yr⁻¹ in the period of 2000–2011. Using observations from Mt. Bachelor Observatory, Gratz et al. (2015) also show a negative trend of CO concentration by 1.9 % yr⁻¹ in the period of 2004–2013. However, the reason for the large variation of tropospheric CO abundance is still unclear; for example, Strode et al. (2016) found decreases in modeled CO abundance over North America and

Europe, but increases over China, based on bottom-up emissions.

There is currently much effort focused on accurately quantifying emissions of CO. For fossil fuels and biofuels, energy consumption statistics and emission factors are usually used to construct the emission inventories (e.g., Streets et al., 2006; Ohara et al., 2007; Zhang et al., 2009; Zhao et al., 2012). Biomass burning emissions are commonly calculated as the product of burned area, fuel loads, combustion completeness and emission factors (e.g., van der Werf et al., 2006, 2010; van Leeuwen and van der Werf, 2011). Because of the large uncertainties in the emission inventories, space-based remotely sensed measurements and surface/aircraft in situ observations have been assimilated to provide “top-down” constraints on CO emissions (e.g., Arelano et al., 2006; Chevallier et al., 2009; Jones et al., 2009; Kopacz et al., 2010; Jiang et al., 2011; Fortems-Cheiney et al., 2011; Hooghiemstra et al., 2012; Miyazaki et al., 2015). In a recent study, Yin et al. (2015) constrained global CO emissions for the period 2002–2011 to investigate the possible reasons for the decreasing CO abundance in the Northern Hemisphere. Using MOPITT column data (version V6J) over the whole globe, Yin et al. (2015) indicate that the negative trend of tropospheric CO abundance in the Northern Hemisphere is driven by decreasing anthropogenic emissions from North America, Europe and China.

The major sink of tropospheric CO is OH. Because of its high variability and short lifetime (about 1 s), it is difficult to assess the spatial and temporal variation of global OH through direct measurements (Spivakovsky et al., 2000; Lelieveld et al., 2004). Alternatively, Montzka et al. (2011) demonstrated small interannual variability of global OH for the period 1997–2007 by using the loss rate of methyl chloroform (MCF) as a proxy. The measurements of MCF have been assimilated in recent CO inversion studies to provide updated OH (e.g., Fortems-Cheiney et al., 2011, 2012; Yin et al., 2015), but the estimates are adversely affected by the sparse distribution of measurements.

The objective of this work is to investigate the dominant reasons for the decreasing CO trend in the Northern Hemisphere and to provide updated CO emission estimates for model studies. Using methods and results from our prior work, our approach is intended to reduce the effects of model errors of transport and chemistry, as well as bias errors in the data, on our conclusions about CO emissions. These are the primary uncertainties that affect CO emissions estimates. For example, bias errors in MOPITT data can have a substantial impact on emissions estimates (Deeter et al., 2014). Model errors of transport and chemistry will have variable and substantial effects on CO emissions in different parts of the globe due to seasonal and latitudinal variations in convection, advection and boundary layer height (Jiang et al., 2013, 2015a, b).

In order to reduce the influences from these measurement and model transport systematic errors, we performed

a two-step inversion by combining sequential Kalman filter (Jiang et al., 2013, 2015a, b) with four-dimensional variational (4D-Var) assimilation (Henze et al., 2007) in this work, using the GEOS-Chem model. Instead of optimizing the CO concentrations and emissions simultaneously (e.g., Fortems-Cheiney et al., 2011, 2012; Yin et al., 2015), our first step, the sequential Kalman filter, modifies the atmospheric CO concentration directly to provide low-bias initial (monthly) and boundary (hourly) conditions, whereas the second step (4D-Var) constrains CO emissions assuming perfect initial and boundary conditions. We also apply bias corrections to MOPITT and compare the surface CO concentrations obtained by constraining the model with MOPITT profile, total column or lower-tropospheric CO data to test which data type provides the most accurate comparison with independent surface in situ measurements.

This paper is organized as follows: in Sect. 2 we describe the MOPITT instruments and the GEOS-Chem model used in this work. In Sect. 3 we outline the inverse method. We then investigate the long-term variations of global tropospheric OH and CO emissions in Sect. 4, and we discuss the changes in tropospheric CO and the contributions from emissions and meteorological conditions. Our conclusions follow in Sect. 5.

2 Observations and model

2.1 MOPITT

The MOPITT instrument was launched on 18 December 1999 on the NASA/Terra spacecraft. The satellite is in a sun-synchronous polar orbit of 705 km and crosses the Equator at 10:30 local time. The instrument makes measurements in a 612 km cross-track scan with a footprint of 22 km × 22 km and provides global coverage every 3 days. The MOPITT data used here were obtained from the joint (J) retrieval (V6J) of CO from thermal infrared (TIR, 4.7 μm) and near-infrared (NIR, 2.3 μm) radiances using an optimal estimation approach (Worden et al., 2010; Deeter et al., 2011). The retrieved volume mixing ratios (VMRs) are reported as layer averages of 10 pressure levels (surface, 900, 800, 700, 600, 500, 400, 300, 200 and 100 hPa). The relationship between the retrieved CO profile and the true atmospheric state can be described as

$$\hat{z} = z_a + \mathbf{A}(z - z_a) + \mathbf{G}\epsilon, \quad (1)$$

where z_a is the MOPITT a priori CO profile; z is the true atmospheric state; $\mathbf{G}\epsilon$ describes the retrieval error; and $\mathbf{A} = \partial\hat{z}/\partial z$ is the MOPITT averaging kernel matrix, which gives the sensitivity of the retrieval to the actual CO in the atmosphere. The MOPITT V6 data have been evaluated by Deeter et al. (2014) using aircraft measurements from HIPPO and the National Oceanic and Atmospheric Administration (NOAA). For the

TIR/NIR multi-spectral retrievals, they found negative bias drift ($-1.27\% \text{ yr}^{-1}$) in the lower troposphere (800 hPa) and positive bias drift ($1.64\% \text{ yr}^{-1}$) in the upper troposphere (200 hPa). The bias drift in the total column is negligible ($0.15\% \text{ yr}^{-1}$). Following our previous studies (Jiang et al., 2013, 2015a, b), we reject MOPITT data with CO column amounts less than $5 \times 10^{17} \text{ molec cm}^{-2}$ and with low-cloud observations. The threshold of $5 \times 10^{17} \text{ molec cm}^{-2}$ was selected to prevent unrealistically low CO columns from adversely impacting the inversion analyses. Since the NIR radiances measure reflected solar radiation, only daytime data are considered.

Figure 1 shows the comparison between MOPITT CO retrievals and HIPPO aircraft measurements. The aircraft measurements are smoothed with MOPITT averaging kernels to make it more comparable, as the aircraft measurements have high vertical resolution. The comparison demonstrates a negative bias of MOPITT CO retrievals in the tropics and a positive bias at the middle latitudes in the lower troposphere. Opposite bias is observed in the upper troposphere. Similar latitude-dependent biases in remote-sensing retrievals have been revealed for methane (CH_4) observations from Scanning Imaging Absorption Spectrometer for Atmospheric Chartography (SCIAMACHY; Bergamaschi et al., 2007, 2009; Meirink et al., 2008), Greenhouse Gases Observing Satellite (GOSAT; Turner et al., 2015) and CO observation from MOPITT (version 4; Hooghiemstra et al., 2012). Similar to previous studies, we reduce the adverse effect of the latitude-dependent bias by applying latitude-dependent correction factors to MOPITT CO retrievals, based on the black solid line in Fig. 1, which represents a 4-order polynomial curve fitting (in a least-squares sense) for all data points. It should be noted that we are only correcting for a time-invariant latitudinal and vertical dependence of MOPITT CO bias. Seasonal and interannual variations of MOPITT retrieval biases are not corrected due to the limited spatial sampling of in situ data available for determining retrieval bias changes over the MOPITT data record (Deeter et al., 2014). The remaining bias drifts have implications for interpreting the CO emission trends derived from total column vs. profile or lower-tropospheric profile.

2.2 GEOS-Chem

The GEOS-Chem global chemical transport model (CTM) (www.geos-chem.org) is driven by assimilated meteorological fields from the NASA Goddard Earth Observing System (GEOS-5) at the Global Modeling and data Assimilation Office. For the simulations in this work, various versions of GEOS meteorological fields are used, including GEOS-4 (2000–2003), GEOS-5 (2004–2012) and GEOS-FP (2013–2015). We use version v35j of the GEOS-Chem adjoint, which is based on v8-02-01 of the forward GEOS-Chem model, with relevant updates through v9-02-01. Our analysis is conducted at a horizontal resolution of $4^\circ \times 5^\circ$ with 47 ver-

tical levels and employs the CO-only simulation in GEOS-Chem, which uses archived monthly OH fields from the full-chemistry simulation. The OH fields used in this work are from GEOS-Chem version v5-07-08, with a global annual mean OH concentration of $0.99 \times 10^6 \text{ molec cm}^{-3}$ (Evans and Jacob, 2005). The potential long-term variation of global tropospheric OH is evaluated in Sect. 4.

The global anthropogenic emission inventory is from EDGAR 3.2FT2000 (Olivier and Berdowski, 2001) but has been replaced by the following regional emission inventories: the US Environmental Protection Agency (EPA) National Emission Inventory (NEI) for 2008 in North America, the Criteria Air Contaminants (CAC) inventory for Canada, the Big Bend Regional Aerosol and Visibility Observational (BRAVO) Study Emissions Inventory for Mexico (Kuhns et al., 2003), the Cooperative Program for Monitoring and Evaluation of the Long-range Transmission of Air Pollutants in Europe (EMEP) inventory for Europe in 2000 (Vestreng and Klein, 2002) and the INTEX-B Asia emissions inventory for 2006 (Zhang et al., 2009). Biomass burning emissions are based on the Global Fire Emission Database (GFED3; van der Werf et al., 2010). The a priori biomass burning emissions in September–November 2006 were applied to September–November 2015 over Indonesia. Additional CO sources come from oxidation of methane and biogenic volatile organic compounds (VOCs) as described in previous studies (Kopacz et al., 2010; Jiang et al., 2013). The biogenic emissions are simulated using the Model of Emissions of Gases and Aerosols from Nature, version 2.0 (MEGANv2.0; Guenther et al., 2006). The distribution of the annual mean CO emissions for 2001–2015 is shown in Fig. 2. The annual global sources are 892 Tg CO from fossil fuel, biofuel and biomass burning; 623 Tg CO from the oxidation of biogenic VOCs; and 876 Tg CO from the oxidation of CH_4 .

3 Inversion approach

We use the 4D-Var data assimilation system in GEOS-Chem (Henze et al., 2007) to constrain the CO sources. In this approach, we minimize the cost function defined as

$$J(\mathbf{x}) = \sum_{i=1}^N [\mathbf{F}_i(\mathbf{x}) - \mathbf{z}_i]^T \mathbf{S}_\Sigma^{-1} [\mathbf{F}_i(\mathbf{x}) - \mathbf{z}_i] + (\mathbf{x} - \mathbf{x}_a)^T \mathbf{S}_a^{-1} (\mathbf{x} - \mathbf{x}_a), \quad (2)$$

where \mathbf{x} is the state vector of CO emissions, N is the number of MOPITT observations that are distributed in time over the assimilation period, \mathbf{z}_i is a given MOPITT measurement and $\mathbf{F}(\mathbf{x})$ is the forward model. The temporal resolution of forward-model output ($\mathbf{F}(\mathbf{x})$) is 1 h, and consequently the high-resolution MOPITT measurements are averaged temporally (1 h resolution) and spatially ($4^\circ \times 5^\circ$ resolution) to produce grid mean observations. The number (N) of grid mean observations in our assimilation window (1 month) is around 10 000.

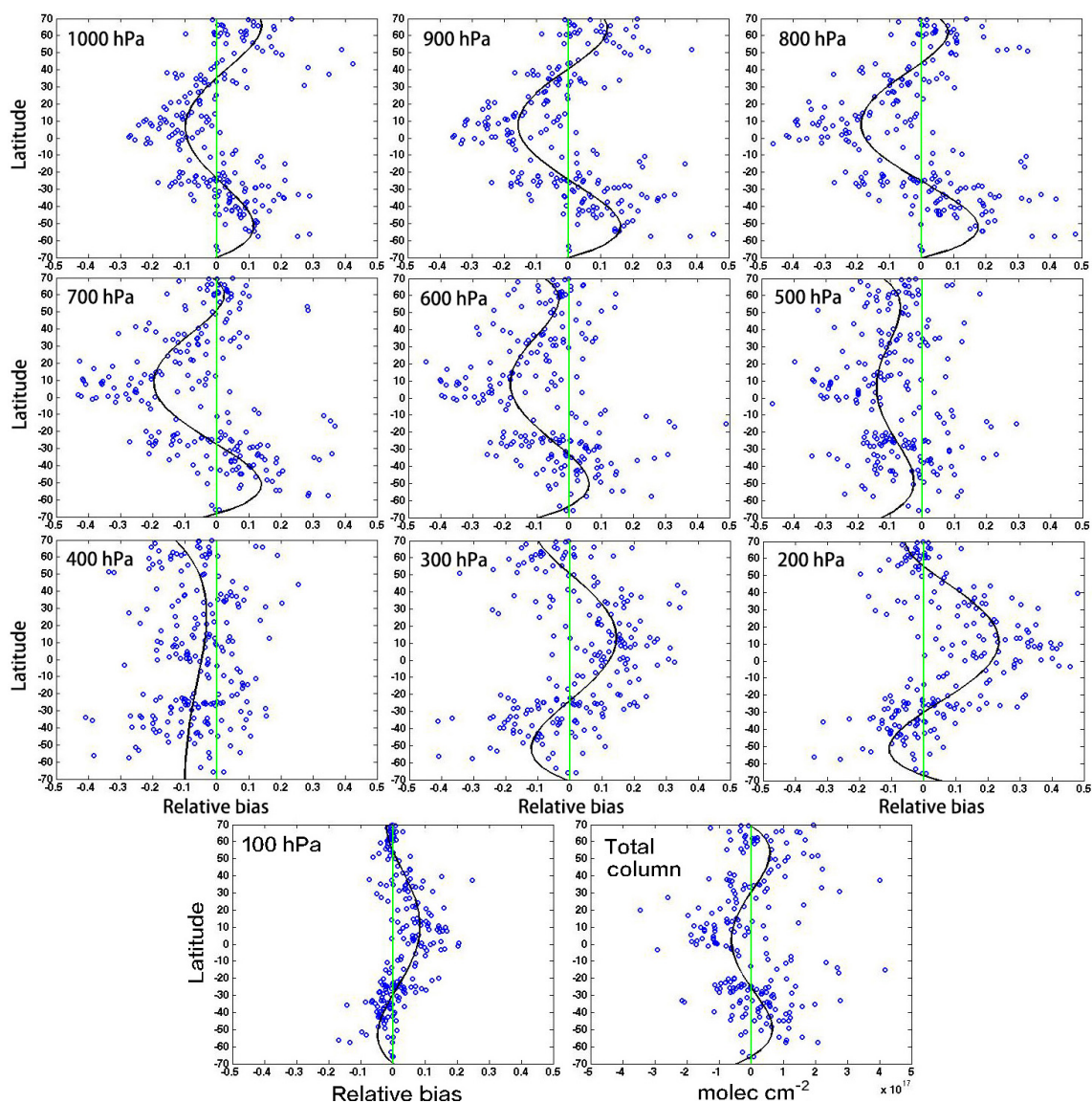


Figure 1. Difference between MOPITT CO retrievals and HIPPO aircraft measurements. The aircraft measurements are smoothed with MOPITT averaging kernels. The black solid line shows the 4-order polynomial curve fitting which is used to correct MOPITT data in this work.

The error estimates are assumed to be Gaussian and are given by \mathbf{S}_{Σ} , the observational error covariance matrix, and \mathbf{S}_a , the a priori error covariance matrix. The Gaussian assumption excludes important systematic errors, such as biases in OH distribution, long-range transport and satellite retrievals in the cost function. Due to a lack of meaningful information about the systematic errors, we assume a uniform observation error of 20 % without spatial correlation following our previous studies (Jiang et al., 2011, 2013, 2015a, b). As shown in Fig. S1 (see Supplement), we expect limited influences from the assumption of uniform observation error. The combustion CO sources (fossil fuel, biofuel and biomass burning) and the oxidation source from biogenic VOCs are

combined together, assuming a 50 % uniform a priori error. We optimize the source of CO from the oxidation of CH_4 separately as an aggregated global source, assuming an a priori uncertainty of 25 %.

The a posteriori error covariance matrix is the inverse of the Hessian matrix, which is not stored in the 4D-Var optimization scheme. Boussez et al. (2015) presented an approach to construct the a posteriori error covariance matrix using the approximation of the Hessian matrix. As opposed to earlier studies using surface measurements, the high spatial density of measurements from satellite instruments can effectively suppress the contribution from random errors in the cost function, leaving systematic errors as the critical fac-

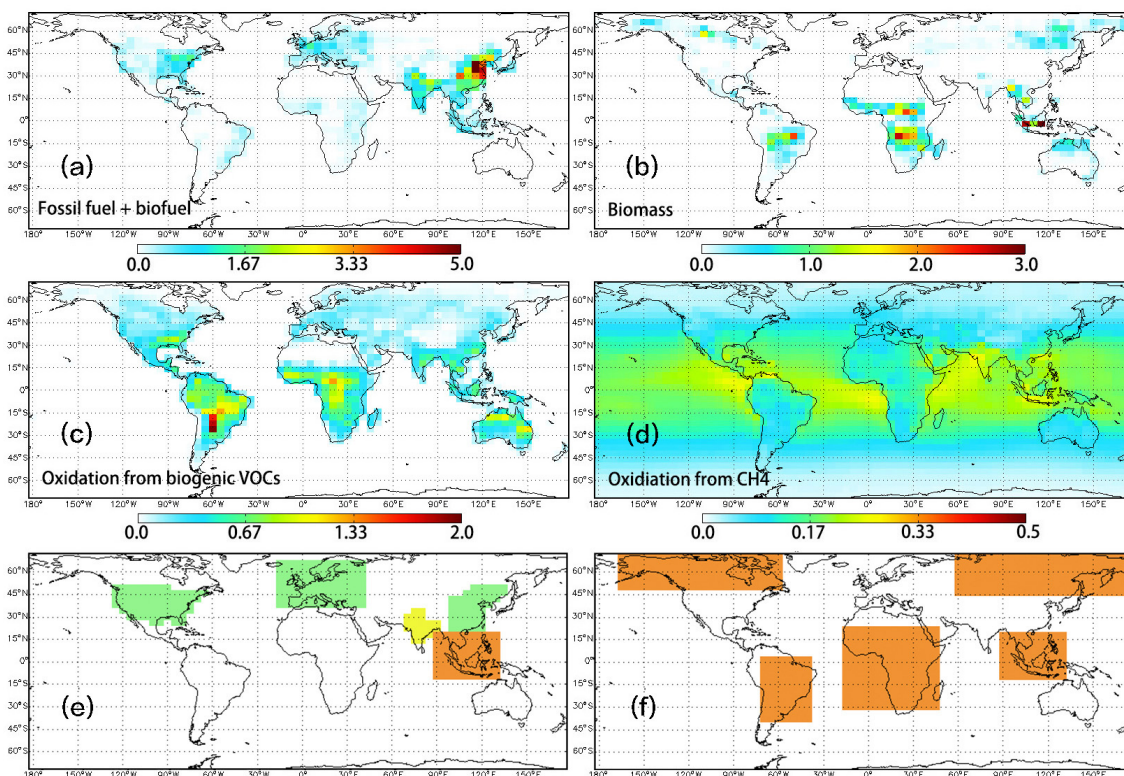


Figure 2. (a–d) Mean a priori CO emissions from combustion sources and the oxidation of biogenic VOCs and CH₄ from 2001 to 2015. The unit is 10^{12} molec cm⁻² s⁻¹. (e–f) Region definitions for (e) anthropogenic and (f) biomass burning sources.

tor in the uncertainty. As shown by Heald et al. (2004), different assumptions about the inversion configuration (systematic errors) can produce differences in the source estimates that are significantly larger than the a posteriori errors calculated based on random errors. Consequently, estimates of a posteriori uncertainties are not provided in this work (e.g., Tables 1 and 2).

Removing the bias in initial conditions is essential for inverse analysis (Jiang et al., 2013) and can be performed with various data assimilation techniques. Model simulations driven by optimized emissions can provide good initial conditions (e.g., Gonzi et al., 2011; Bruhwiler et al., 2014; Deng et al., 2014; Houweling et al., 2014). Alternatively, tracer concentrations can be modified directly to avoid the effect from long-range-transport error (e.g., Kopacz et al., 2009; Jiang et al., 2013, 2015a). There are also efforts to optimize emissions and concentrations simultaneously (e.g., Fortems-Cheiney et al., 2011, 2012; Bergamaschi et al., 2013; Yin et al., 2015); however, the contributions from emissions and concentrations to model bias may be hard to distinguish. Figure 3 shows the methodology of our assimilation system. Following our previous studies (Jiang et al., 2013, 2015a, b), we produce initial conditions at the beginning of each monthly assimilation window by assimilating MOPITT data using a sequential Kalman filter. For the results presented

here, the Kalman filter assimilation was carried out from 1 March 2000 to 31 December 2015.

Systematic model errors have a critical influence on inverse analysis. Jiang et al. (2013) found that the modeled CO concentrations from a 10-day forecast simulation have large discrepancy with assimilated CO fields, because of bias in model convective transport. Jiang et al. (2015a) demonstrated that free-tropospheric CO is more susceptible to the influence of OH bias than lower-tropospheric CO due to the process of long-range transport. Previous studies suggest the influences of systematic errors can be mitigated by enhancing the contributions from local emissions to the discrepancy between model and data, while keeping the influence from long-range transport as low as possible due to sources of uncertainties that are difficult to quantify. For example, Pfister et al. (2005) constrained biomass burning CO emissions from boreal North America with optimized CO fields outside the impacted region; Jiang et al. (2015b) indicated that their regional inversions were more reliable when the boundary conditions were optimized.

In this work, we designed a two-step inversion to reduce the effects of these systematic errors. As shown in Fig. 3, we define the ocean scene (red grids) as boundary conditions. In the first step of our inverse analysis, sequential Kalman filter assimilation, we directly modify CO concentrations without

Table 1. Annual total anthropogenic CO emission in different regions, from 2001 to 2015, constrained with MOPITT column, profile and lower-tropospheric data. The region definition is shown in Fig. 2e.

Years	MOPITT Column (Tg yr^{-1})					MOPITT Profile (Tg yr^{-1})					MOPITT Lower Profile (Tg yr^{-1})				
	United States	Europe	E China	India/ SE Asia	Global total	United States	Europe	E China	India/ SE Asia	Global total	United States	Europe	E China	India/ SE Asia	Global total
2001	87.8	71.6	165.7	102.2	526.5	87.7	77.3	170.4	97.5	522.9	112.9	92.0	215.7	136.1	677.5
2002	84.1	65.9	171.3	93.3	508.9	82.3	77.1	176.1	81.1	504.2	110.1	89.8	221.9	119.8	658.2
2003	80.8	65.3	178.8	95.4	516.2	80.4	74.5	189.2	88.5	523.2	103.6	87.0	218.1	121.9	645.1
2004	77.4	65.5	178.5	105.0	524.5	91.1	83.8	205.6	113.8	596.6	103.0	89.5	222.8	124.6	652.7
2005	72.7	64.6	178.6	104.3	518.0	82.6	79.4	200.6	116.8	581.5	92.7	84.5	215.3	126.2	630.6
2006	74.6	61.5	172.7	98.1	500.7	85.6	74.5	197.7	111.0	567.6	93.9	78.9	205.1	118.1	603.1
2007	73.7	56.5	177.1	105.8	511.4	84.0	67.9	200.9	113.2	568.2	90.9	71.8	208.1	119.4	599.6
2008	67.1	55.5	150.2	102.1	473.5	77.2	65.4	175.4	110.2	530.8	83.9	69.6	175.0	111.1	548.4
2009	66.0	54.8	162.0	105.7	486.0	74.5	65.1	185.9	118.3	544.1	78.0	67.0	184.5	115.1	547.4
2010	59.2	54.5	159.3	100.5	470.6	67.8	65.3	183.1	112.8	529.6	73.5	69.0	185.5	106.7	539.1
2011	53.5	52.9	153.2	107.4	461.9	60.5	63.1	179.5	120.3	522.1	63.0	65.6	175.7	107.5	511.0
2012	54.9	58.3	167.0	113.8	496.2	58.2	65.2	184.2	128.8	540.8	62.5	68.9	187.0	115.7	540.7
2013	54.3	62.6	160.4	120.9	503.0	56.7	68.8	171.2	131.3	532.2	61.8	73.8	176.8	114.6	531.5
2014	55.0	60.1	157.1	121.3	499.4	56.8	63.9	175.6	133.4	533.4	60.9	68.5	174.4	115.5	523.5
2015	55.1	61.4	145.1	115.6	484.7	56.8	66.9	159.0	130.4	520.2	59.5	69.3	160.5	109.2	504.3

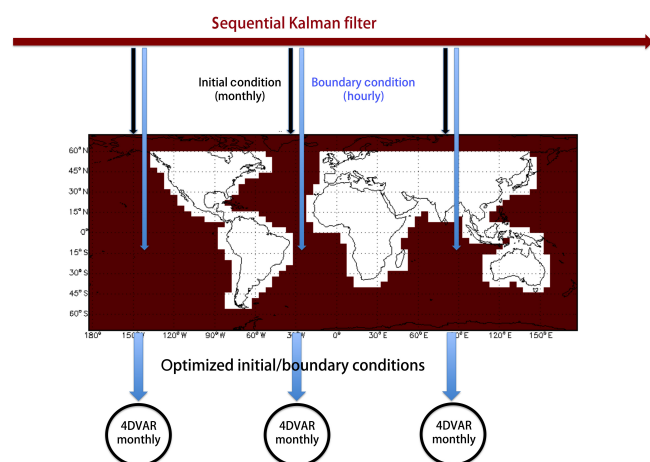


Figure 3. Schematic diagram for methodology of the assimilation system. Sequential Kalman filter was run from 1 March 2000 to 31 December 2015 to produce the optimized initial conditions (monthly) and boundary conditions (hourly). Monthly 4D-Var inversions were performed with the optimized initial conditions. Only MOPITT data over land (white grids) were assimilated in the 4D-Var inversions, while the CO abundances over ocean (red grids) were defined as boundaries and rewritten using the optimized hourly CO fields from the Kalman filter. The Kalman filter run is completely independent of the 4D-Var inversions. There is no feedback of the 4D-Var inversion results to the boundary conditions.

any change to emissions in order to provide optimized CO fields as consistent as possible with MOPITT. In the second step, the optimized CO fields are used to rewrite CO concentrations over the ocean every hour, while 4D-Var inversion is employed to constrain CO emissions, without any change in CO distribution over ocean. Only MOPITT data over land (white grids) were assimilated to constrain CO emissions in the second step. In our previous study (Jiang et al., 2015b),

we performed a regional inversion over the North America continent driven with optimized boundary conditions from global-scale simulation by assimilating MOPITT CO measurements. In this work, we convert the global inversion system to a combination of several regional inversions, and the optimization on the boundary conditions is exactly the same as the regional inversion (Jiang et al., 2015b). With the fixed/optimized boundary conditions, the emission and transport errors from one continent (e.g., North America) will not affect the emission estimation of another continent (e.g., Europe).

4 Results and discussion

4.1 Long-term variation of global tropospheric OH

The distribution of tropospheric OH has significant influence on the inverse analysis of CO emissions (Jiang et al., 2011). Various approaches have been employed to improve the OH distribution in previous studies. Jiang et al. (2013) assimilated MOPITT CO retrievals in a full-chemistry model simulation to provide updated OH fields. Miyazaki et al. (2015) demonstrated that assimilation of Tropospheric Emission Spectrometer (TES) O_3 , Ozone Monitoring Instrument (OMI) NO_2 and MOPITT CO can provide a better description of tropospheric OH. There have also been recent efforts that have assimilated surface in situ MCF measurements (Fortems-Cheiney et al., 2011, 2012; Yin et al., 2015). However, because of the uncertainties in model chemistry schemes, potential bias drifts in satellite measurements and sparse distribution of surface in situ measurements, OH abundances provided by these approaches may not be ideal for the estimation of long-term CO variation.

Emissions of MCF are regulated by the Montreal Protocol agreement. The loss rate of MCF has become a good

Table 2. Annual total biomass burning CO emission in different regions, from 2001 to 2015, constrained with MOPITT column, profile and lower-tropospheric data. The region definition is shown in Fig. 2f.

Years	MOPITT Column (Tg yr^{-1})						MOPITT Profile (Tg yr^{-1})						MOPITT Lower Profile (Tg yr^{-1})									
	Boreal America	Boreal Asia	Boreal America	South America	Africa	SE Asia	Boreal America	Boreal Asia	South America	Africa	SE Asia	Boreal America	Boreal Asia	South America	Africa	SE Asia	Boreal America	Boreal Asia	South America	Africa	SE Asia	Global total
2001	1.2	24.8	25.5	160.8	14.0	272.4	1.2	26.5	28.4	153.5	9.5	267.7	1.3	28.4	31.9	222.0	21.4	369.6				
2002	10.1	23.7	38.4	164.5	44.9	331.5	12.6	50.6	40.7	171.3	36.1	369.2	17.0	65.9	42.1	222.9	67.9	488.3				
2003	8.9	47.7	39.6	162.7	17.2	324.2	11.1	65.4	41.4	174.9	14.1	356.2	13.6	76.9	44.0	220.9	24.8	445.2				
2004	12.7	4.7	55.3	136.9	39.5	292.3	26.9	5.9	58.4	158.6	44.4	350.1	46.3	6.8	55.7	167.1	46.7	381.1				
2005	11.2	7.7	61.8	167.4	29.4	318.4	15.5	9.8	67.3	193.3	31.1	364.9	19.1	11.3	68.1	203.1	34.8	387.3				
2006	4.5	11.5	32.9	134.0	51.0	278.0	5.4	14.3	36.3	158.1	68.4	337.6	5.8	15.4	32.9	164.6	77.9	354.9				
2007	5.1	10.2	72.9	154.9	19.3	313.4	5.9	12.8	84.6	174.3	23.9	365.8	6.6	13.8	78.4	182.1	23.7	369.3				
2008	3.6	19.5	26.9	151.9	10.9	245.9	4.0	25.3	31.1	176.2	13.5	288.4	4.9	26.2	31.3	174.8	13.4	290.4				
2009	5.4	11.1	16.4	132.8	36.7	254.8	5.7	12.8	16.9	142.2	37.3	274.1	6.1	13.2	16.8	139.5	38.3	274.2				
2010	7.5	13.0	61.8	150.5	15.1	281.9	10.4	16.8	72.4	168.1	20.2	329.1	11.4	19.5	69.1	167.3	20.4	329.6				
2011	4.1	13.3	15.1	145.7	11.5	240.3	5.1	15.8	16.6	153.0	15.4	261.5	5.6	16.1	16.3	145.4	13.4	250.8				
2012	4.8	15.3	24.9	143.7	13.8	256.1	5.1	16.6	25.5	151.9	16.9	275.6	5.8	17.0	26.5	154.4	16.9	277.1				
2013	4.5	11.7	12.4	172.0	13.1	257.6	6.0	12.9	13.9	170.8	22.7	270.1	6.7	13.8	16.0	187.0	14.6	284.4				
2014	6.8	13.9	17.9	167.0	21.4	275.4	8.1	15.4	17.3	161.1	25.8	275.6	7.4	15.3	18.6	181.3	19.8	289.6				
2015	7.0	14.3	29.3	193.6	66.4	357.7	7.4	15.3	28.0	188.9	162.0	448.1	6.8	14.3	28.1	204.0	87.1	386.5				

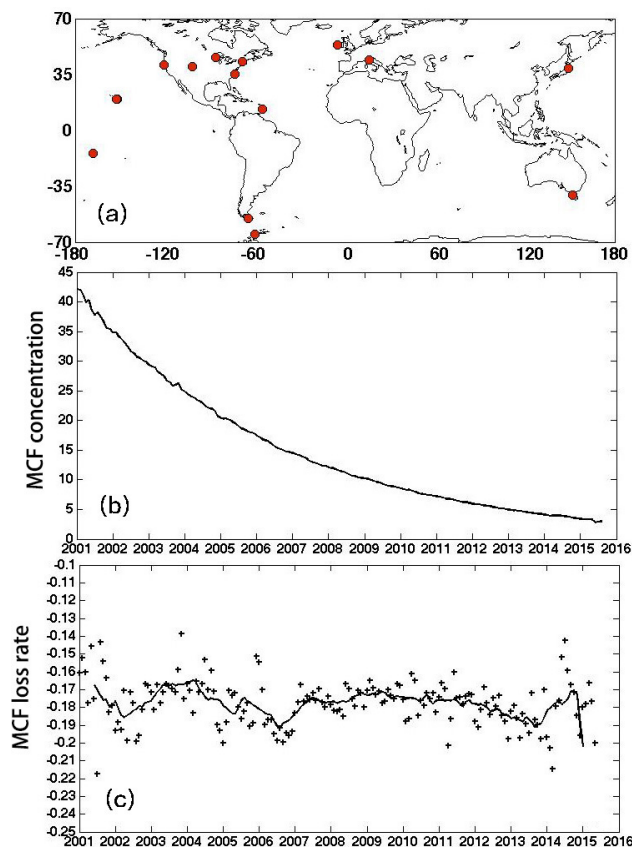


Figure 4. (a) Locations of WDCGG sites with MCF measurements. (b) Global mean MCF concentration. (c) Exponential loss rate of MCF, derived from the 12-month difference of monthly means (e.g., $\ln(\text{MCF}_{\text{Jan2007}}/\text{MCF}_{\text{Jan2006}})$). The black solid line shows the 12-month mean value.

tool for evaluating the variation of tropospheric OH (e.g., Krol et al., 1998; Bousquet et al., 2005; Prinn et al., 2005; Montzka et al., 2011). Using the same approach as Montzka et al. (2011), we assess the variation of tropospheric OH in the period of 2001–2015. Figure 4a shows the locations of World Data Centre for Greenhouse Gases (WDCGG) sites with MCF measurements, and Fig. 4b shows the global mean MCF concentration in the past 15 years. Similar as Montzka et al. (2011), our result shows an exponential decrease of MCF concentration. The loss rate of MCF, derived from the 12-month difference of monthly means (e.g., $\ln(\text{MCF}_{\text{Jan2007}}/\text{MCF}_{\text{Jan2006}})$), varied by 0.2% in the past 15 years (Fig. 4c). The interannual variation is more likely due to the sparsity and discontinuity of measurements. It should be noted that the MCF measurements in the period middle 2008–middle 2009 are subject to some small biases owing to instrumental issues; however, we believe its influence on our analysis (2001–2015) is small.

The small loss rate variation of MCF demonstrates that the long-term variation of global mean OH distributions is negligible in the past 15 years. Consequently, the decreasing

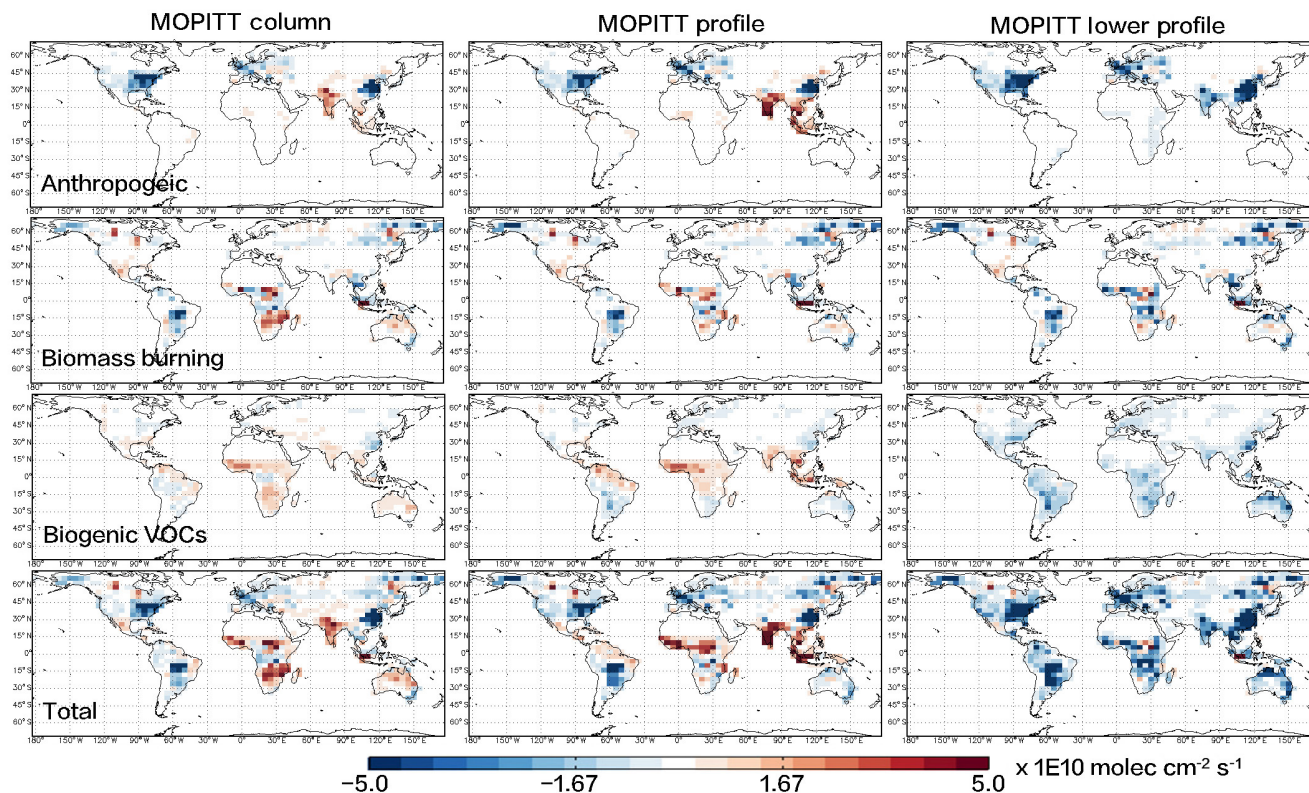


Figure 5. CO emission trends for 2001–2015 constrained with MOPITT column, profile and lower-tropospheric profile data. The months dominated by biomass burning emissions are excluded from the trend calculation for anthropogenic and biogenic VOC emissions.

trend of tropospheric CO in North Hemisphere is driven by decreasing CO sources, rather than sinks. For this reason, the default monthly OH fields of the GEOS-Chem model (Evans et al., 2005), without interannual variability, are used in this work to constrain the long-term variation of CO emissions. A previous study (Krol et al., 1998) has indicated a small discrepancy between derived OH trends based on MCF measurements due to various methods. Because the abundances of tropospheric OH have large regional discrepancies (e.g., Jiang et al., 2015a), it is possible that the actual OH is more variable in regions lacking MCF measurements (e.g., India and southeast Asia). Furthermore, the magnitude and seasonality of the default monthly OH fields could also have uncertainty. Consequently, the magnitude of CO emissions in our analysis may still be affected by biases in OH, although the two-step assimilation system is designed to suppress their influence.

4.2 Long-term variation of global CO emissions

In this work, we performed monthly inversions for the period of 2001–2015, using MOPITT column, profile and lower-tropospheric profile (lowest three retrieval levels) data to investigate the influences associated with vertical sensitivity of satellite instrument and model transport error. Figure 5

shows the CO emission trends for 2001–2015 constrained by these different data sets. Because of the combination of various emission categories (i.e., anthropogenic, biomass burning and VOC oxidation) in our methodology, we cannot completely separate the a posteriori emission estimates from different sources. However, the various spatial and temporal distribution of emissions sources (e.g., anthropogenic vs. biomass burning) provides valuable information with which to distinguish the contribution from each category. In order to further isolate the influences of biomass burning, the months dominated by biomass burning (biomass burning CO > 50 % of total CO emission in an individual grid) are excluded in the trend analysis for anthropogenic and VOC sources (Fig. 5).

For anthropogenic sources, all three analyses show significant emission reduction from North America, Europe and China. The emission estimates constrained with MOPITT column and profile data suggest increasing CO emissions from India and southeast Asia. Conversely, the emission estimate constrained with MOPITT lower-tropospheric profile data shows a decreasing trend in this region, and this decreasing trend is also obtained by Yin et al. (2015). In addition to differences in emissions trends expected for the lower-tropospheric profile results due to the negative bias drift in MOPITT lower-tropospheric retrievals (Deeter et al., 2014), we also expect the full MOPITT profile to provide a stronger

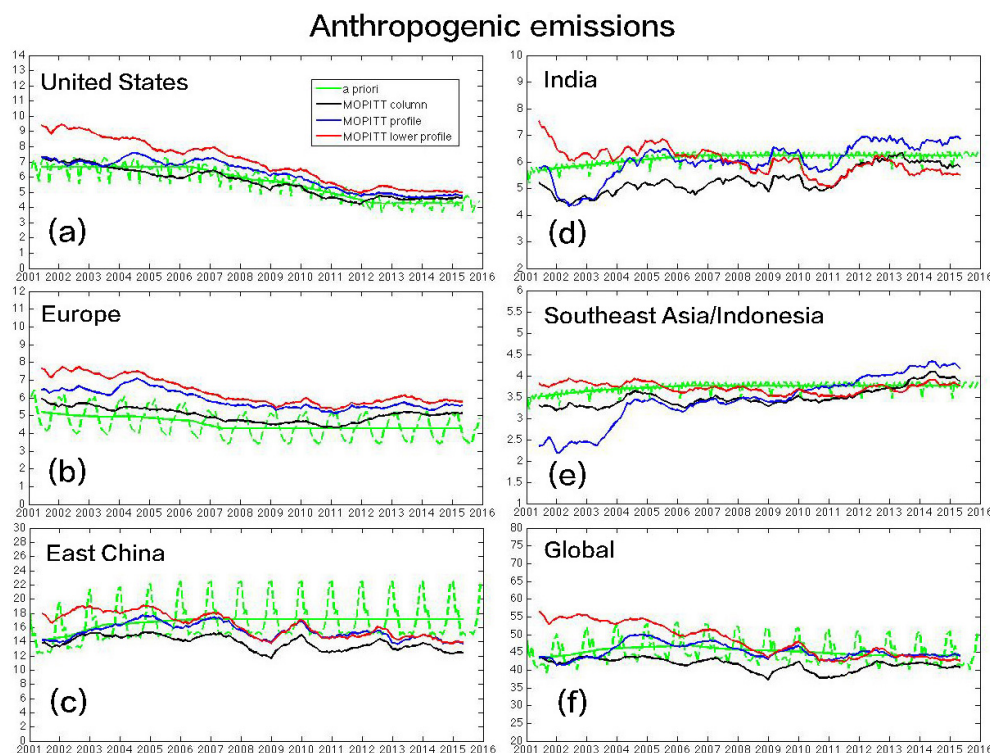


Figure 6. 12-month mean value of anthropogenic CO emissions (with unit Tg month^{-1}) for 2001–2015: a priori emission (green) and a posteriori emissions constrained with MOPITT column data (black), MOPITT profile data (blue) and MOPITT lower-tropospheric profile data (red). The green dash line shows the monthly a priori anthropogenic CO emissions. The region definition is shown in Fig. 2e.

constraint in this region, where errors in model convection can have a large effect on CO emissions estimates (Jiang et al., 2013).

For biomass burning sources, we found a negative trend over boreal North America, boreal Asia and South America, and a positive trend over Indonesia that is primarily due to the strong impacts of El Niño in 2006 and 2015 on biomass burning in this region (e.g., Field et al., 2016). Our results for biogenic VOCs are inconclusive; the emission estimates constrained with MOPITT column and profile data show moderate positive trends in the tropics and slight negative trends in midlatitude regions, whereas the emission estimate constrained with MOPITT lower-tropospheric profile data shows a negative trend globally.

4.2.1 Regional analysis for anthropogenic emissions

Figure 6a shows the regional variation of anthropogenic emissions from the United States (US). The emission estimates constrained with MOPITT column and profile data match very well with the a priori emissions, whereas the emission estimate constrained with MOPITT lower-tropospheric profile data is much higher. All three analyses demonstrate a significant emission reduction over our study period. As shown in Table 1, the total anthropogenic CO emission (constrained with MOPITT

profile data) from the US is 56.8 Tg in 2015, which is 35 % lower than that in 2001 (87.7 Tg). Figure 7a shows the monthly mean CO concentrations from WDCGG stations in the US, which demonstrate a similar decreasing trend to our analysis. The initial increase in 2001–2002 could be caused by uncertainties in the data. The decreasing trend is consistent with the US EPA Emissions Trends Data (<https://www.epa.gov/air-emissions-inventories/air-pollutant-emissions-trends-data>) and other observation records for the western US (Gratz et al., 2015), southeastern US (Hidy et al., 2014) and North Atlantic (Kumar et al., 2013).

Figure 6b shows the regional variation of anthropogenic emissions from Europe. All three analyses show an underestimation of a priori emissions, suggesting the CO emissions in the EMEP inventory are too low. Our results show that anthropogenic emissions decreased during the period of 2001–2007 but were almost unchanged in the following years, which is consistent with the observations from WDCGG stations (Fig. 7b). Recent studies (Hilboll et al., 2013; Schneider et al., 2015) have shown that NO_2 over Europe from SCIAMACHY decreased in the period of 2002–2008 and remained almost unchanged in the period of 2008–2011. Henschel et al. (2015) indicated that the unchanged NO_2 over Europe could be caused by European emissions that are failing

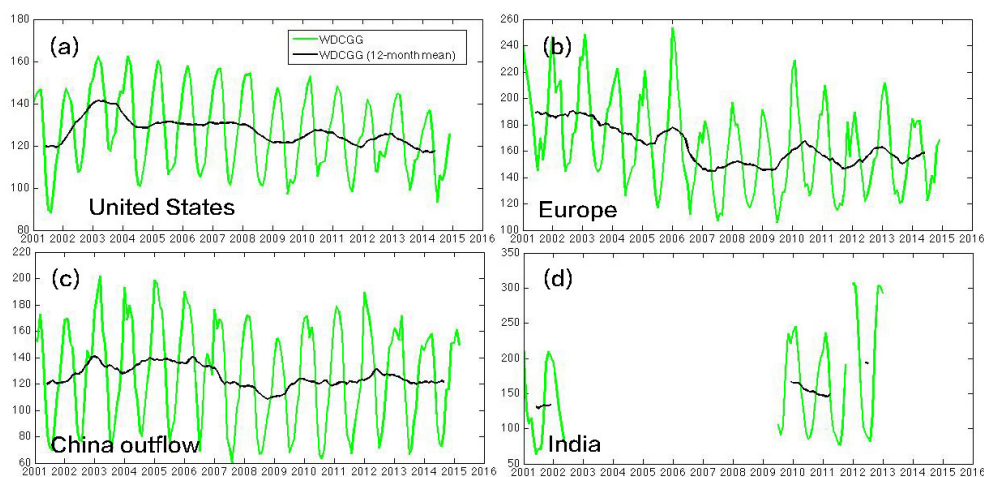


Figure 7. Monthly mean CO concentrations (green) and 12-month mean value (black) from WDCGG stations for 2001–2015. (a) 15-station average in the United States; (b) 20-station average in Europe; (c) 2-station (YON and Minamitorishima (MNM)) average in east China outflow; (d) Cape Rama (CRI) in India.

to achieve the expected reduction standards. Because anthropogenic CO and NO₂ share some of the same combustion sources, it is possible that the unchanged CO emission in our analysis is also due to a failure of emission controls.

Figure 6c shows the regional variation of anthropogenic emissions from east China. We found Chinese anthropogenic emissions to have been increasing in the period of 2001–2004. Accompanied with the global economy recession, the total anthropogenic CO emission (constrained with MOPITT profile data) from east China decreased to 175.4 Tg in 2008, which is 15 % lower than that in 2004 (205.6 Tg). Our analysis shows a temporary increase of Chinese emissions in 2009 (185.9 Tg), followed by continuous decrease. The total Chinese anthropogenic CO emission was 159.0 Tg in 2015, which is 7 % lower than that in 2001 (170.4 Tg). Using surface in situ measurements at Hateruma Island, Tohjima et al. (2014) constrained CO emissions from China for the period 1999–2010. They found that Chinese CO emission increased from 1999 to 2004 and decreased has since 2005. Using a “bottom-up” approach, recent studies (Zhao et al., 2012; Xia et al., 2016) have indicated that the growth trend of Chinese CO emissions has changed since 2005 because of improvements in energy efficiency and emission control regulations (e.g., Liu et al., 2015). Figure 7c shows the observation records from two stations in the east China outflow region, which demonstrate similar variations.

Figure 6d–e show the regional variation of anthropogenic emissions from India and southeast Asia. The emission estimates constrained with MOPITT column and profile data demonstrate a significant positive trend in our study period, whereas the emission estimate constrained with MOPITT lower-tropospheric profile data shows a decreasing trend. Schneider et al. (2015) showed that NO₂ over south Asia from SCIAMACHY increased in the period of 2003–2011.

Using OMI NO₂ measurements, recent studies (e.g., Duncan et al., 2016) have demonstrated that NO₂ over India had a positive trend during 2005–2015. Observations from Cape Rama (CRI) station (Fig. 7d) demonstrate that CO concentration in 2010–2013 was significantly higher than that in 2001–2002. For these reasons, we have more confidence in our results that indicate increasing anthropogenic CO emissions from India and southeast Asia in the past 15 years. The trend based on the MOPITT lower-tropospheric data is incorrect because of errors in modeled convection for this region and the negative bias drift in MOPITT lower-tropospheric retrievals (Deeter et al., 2014). The total anthropogenic CO emission (constrained with MOPITT profile data) from India and southeast Asia was 130.4 Tg in 2015, which is 34 % higher than that in 2001 (97.5 Tg). It should be noted that the inconsistency between our analysis and Yin et al. (2015) suggests more studies are needed for robust conclusion about the variation of anthropogenic CO emissions for this region.

Although our inverse analysis (constrained with MOPITT profile data) suggests similar anthropogenic CO emissions from east China in 2008 and 2014, Fig. 7c demonstrates that mean CO concentrations over the outflow region of east China are 6 ppb higher in 2014 than 2008. Our previous study (Jiang et al., 2015c) indicated that anthropogenic emissions from India and southeast Asia have an important influence on pollutant concentrations in the east China outflow region. It is possible that the increase of CO concentration observed by WDCGG stations in this region is caused by the significant increase of anthropogenic CO emission from India and southeast Asia. In the most recent 5 years (2011–2015), our results (constrained with MOPITT profile data) suggest a 20.5 Tg emission reduction from east China and a 10.1 Tg emission increase from India and southeast Asia. Assuming a fixed emission growth rate, projected anthropogenic CO

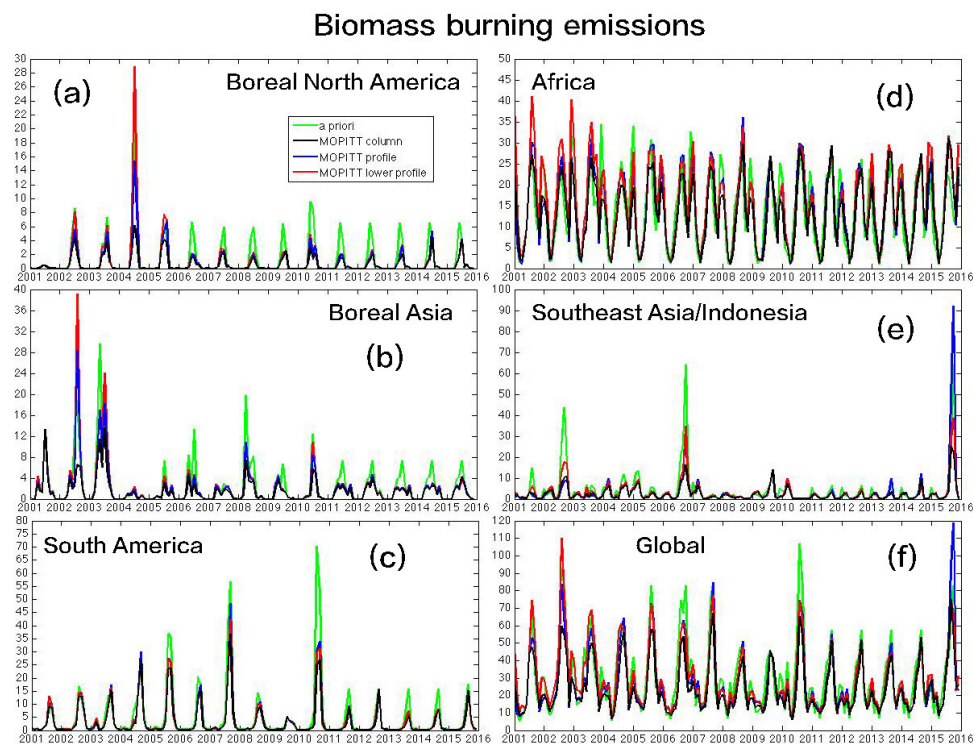


Figure 8. Monthly biomass burning CO emissions (with unit Tg month^{-1}) for 2001–2015: a priori emission (green) and a posteriori emissions constrained with MOPITT column data (black), MOPITT profile data (blue) and MOPITT lower-tropospheric profile data (red). The region definition is shown in Fig. 2f.

emissions from India and southeast Asia will overtake Chinese emissions in 2020, resulting in serious socioeconomic issues on both local and global scales.

4.2.2 Regional analysis for biomass burning emissions

Figure 8 and Table 2 show the regional variation of biomass burning emissions. There are significant decreasing trends in three regions (i.e., boreal North America, boreal Asia and South America). Our results show high biomass burning emissions from boreal North America (mainly Alaska and western Canada) in 2004 (Fig. 8a), which have been reported by previous studies (e.g., Pfister et al., 2005; Turquety et al., 2007), and also from boreal Asia during 2001–2003 (Fig. 8b) due to significant fire activity in Siberia (e.g., Yurganov et al., 2005; Stroppiana et al., 2010). For South America (Fig. 8c), we found higher biomass burning emissions in the periods of 2004–2007 and 2010, consistent with fire activity reported in previous studies (e.g., Hooghiemstra et al., 2012; Bloom et al., 2015).

Figure 8d shows the regional variation of biomass burning emissions from Africa. The fire activities in Africa demonstrate obvious seasonality: peak in boreal winter for northern hemispheric Africa, and in austral winter for southern hemispheric Africa. Similar to previous studies (e.g., Chevallier et al., 2009; Tosca et al., 2015), there is no obvious emission

trend in Africa in the past 15 years. This is also consistent with the burned-area trends described by Andela et al. (2014) which show opposite directions for northern Africa (decreasing) versus southern Africa (increasing) and would have cancelling effects in the trend for the continent as a whole.

Our results exhibit two strong biomass burning events in Indonesia, 2006 and 2015, individually (Fig. 8e). Previous studies (e.g., Logan et al., 2008; Zhang et al., 2011; Worden et al., 2013b; Field et al., 2016) demonstrate the direct relationship between strong Indonesian fires and El Niño. Recent studies (Huang et al., 2014; Inness et al., 2015) confirm low biomass burning activities in Indonesia in the period of 2007–2012. CO emissions from the Indonesian fires associated with the 2015 El Niño were 92 Tg (for October, 2015, as constrained with MOPITT profile data) and were about 3 times higher than the October 2006 El Niño-driven fire emissions (32 Tg). Not including the 2015 El Niño-driven fires, our analysis indicates a negative trend of global biomass burning emissions in the past 15 years, as shown in Fig. 11f.

4.3 Changes in tropospheric CO during 2001–2015

In this section, we evaluate our inversion results using independent long-term surface in situ measurements from WDCGG stations. Figure 9a shows the annual trend of surface CO concentration for 2001–2015 from WDCGG sites and

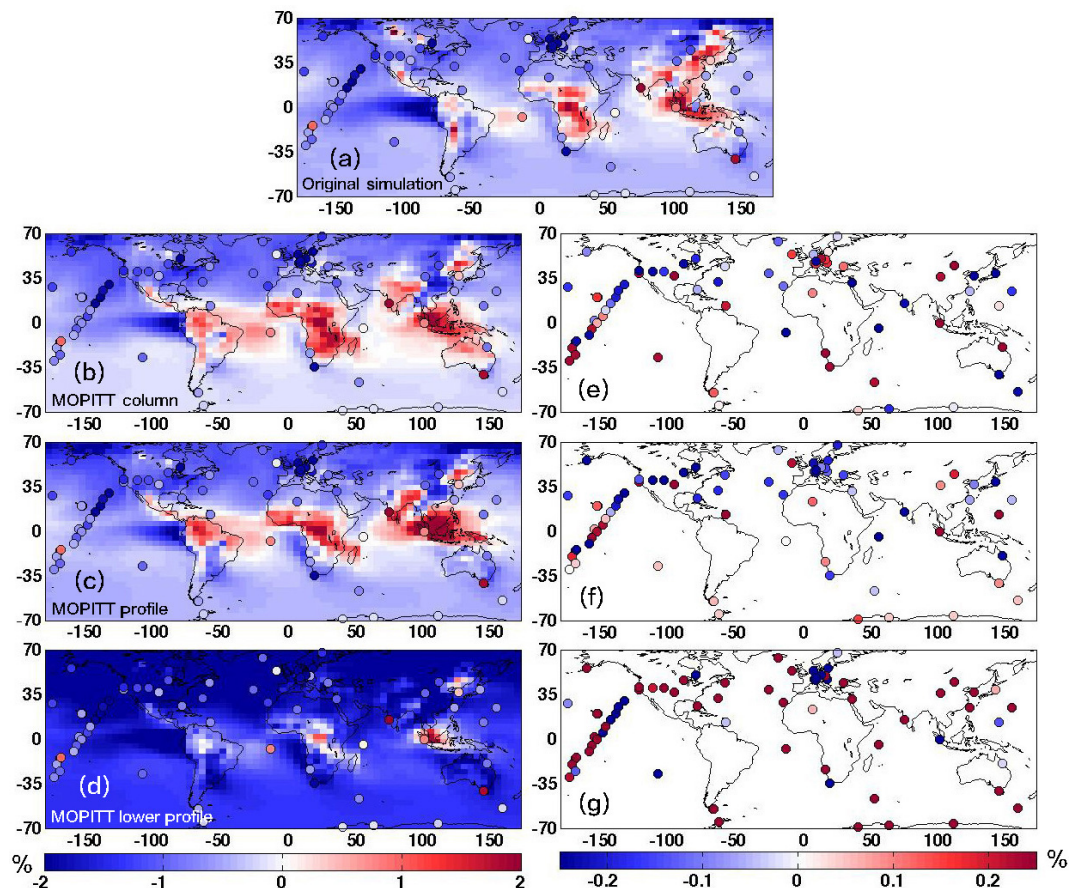


Figure 9. Panels (a–d): long-term trend (annual) of surface CO concentration for 2001–2015 from WDCGG sites, and model simulations driven with a priori and a posteriori emissions. Panels (e–g): effect of a posteriori emissions, derived by $\text{abs}(\text{Trend}_{\text{aposteriori}} - \text{Trend}_{\text{WDCGG}}) - \text{abs}(\text{Trend}_{\text{apriori}} - \text{Trend}_{\text{WDCGG}})$; blue (red) means the a posteriori emissions improves (degrades) the agreement with WDCGG measurements compared to the a priori emissions, while white indicates no change from the priori. Only stations with more than 10-year observations (the time range between the first and last observations) during 2001–2015 are included.

from model simulations driven with a priori emissions. Most WDCGG sites exhibit negative trends in the past 15 years, confirming the decreasing trend of global tropospheric CO, which is consistent with satellite observations (e.g., Warner et al., 2013; Worden et al., 2013a). There are also stations with positive trends, for example, Tae-ahn Peninsula (TAP, Korea), Ascension Island (ASC, equatorial Atlantic Ocean), Cape Rama (CRI, India), Bukit Koto Tabang (BKT, Indonesia) and Cape Grim (CGO, Australia). Globally, the a priori model simulation is in reasonable agreement with WDCGG measurements: both show negative trends at middle/high latitude and positive trends in some tropical regions. However, there are noticeable discrepancies, for example, the surface observation from Yonagunijima (YON, East China Sea) shows a negative trend in our study period, suggesting decreasing trend from Chinese CO emission, whereas the a priori simulation demonstrates a significant positive trend.

Figure 9b–d show the model simulations driven with a posteriori emissions. The a posteriori emissions constrained

with MOPITT lower-tropospheric profile data (Fig. 9d) result in unrealistically large CO reduction, which could be caused by the negative bias drift of MOPITT retrievals in the lower troposphere (Deeter et al., 2014) and the influence from possible variability in model convective transport. The a posteriori emissions constrained with MOPITT column and profile data have similar comparisons. For example, both of them suggest a negative trend over east China, consistent with observations from YON, and positive trend over northeast Asia, consistent with observations from TAP.

In order to better compare the discrepancy between model simulation and surface observations, Fig. 9e–g show the improvement due to a posteriori emissions, derived by $\text{abs}(\text{Trend}_{\text{aposteriori}} - \text{Trend}_{\text{WDCGG}}) - \text{abs}(\text{Trend}_{\text{apriori}} - \text{Trend}_{\text{WDCGG}})$. Blue (red) means the a posteriori emissions improves (degrades) the agreement with WDCGG measurements compared to the simulated surface CO using a priori emissions, while white indicates no change from the prior. As shown in Fig. 9f, the CO emissions constrained

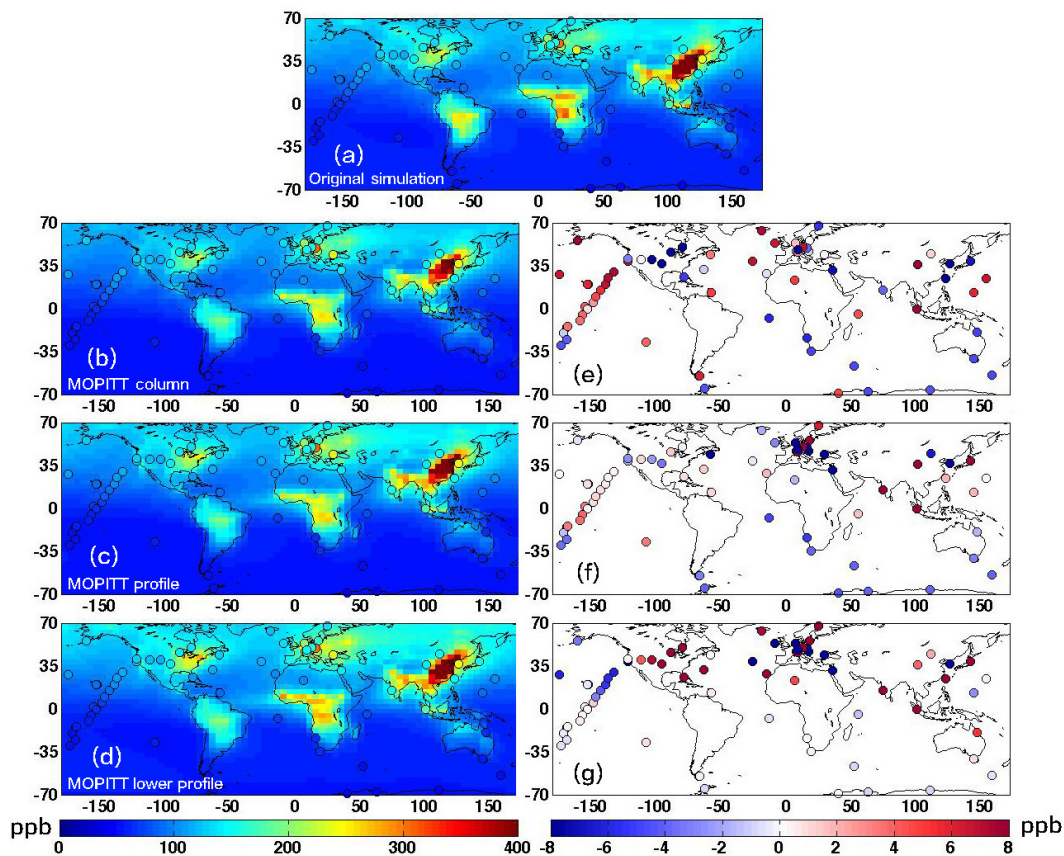


Figure 10. Panels (a–d): long-term mean value of surface CO concentration for 2001–2015 from WDCGG sites, and model simulations driven with a priori and a posteriori emissions. Panels (e–g): effect of a posteriori emissions, derived by $\text{abs}(\text{CO}_{\text{aposteriori}} - \text{CO}_{\text{WDCGG}}) - \text{abs}(\text{CO}_{\text{apriori}} - \text{CO}_{\text{WDCGG}})$; blue (red) means the a posteriori emissions improves (degrades) the agreement with WDCGG measurements compared to the a priori emissions, while white indicates no change from the priori. Only stations with more than 10-year observations (the time range between the first and last observations) during 2001–2015 are included.

with MOPITT profile data improved the model simulation for most WDCGG sites in the Northern Hemisphere. The a posteriori emissions constrained with MOPITT column data are worse, particularly over Europe, while CO emissions constrained with MOPITT profile data over Europe give improved comparisons to WDCGG surface CO measurements. Worden et al. (2010) demonstrated that the degrees of freedom for signal (DFS) of MOPITT multi-spectral profile retrievals (TIR + NIR) is about 1.5–2.0 over land, which is reduced to about 1 DFS when converted to a total column. This reduction in vertical information in MOPITT column data can affect the reliability of inverse analysis results (Jiang et al., 2015a). It should be noticed that the vertical correlation in model simulation is not considered in our assimilation, which could be another possible reason for this discrepancy.

Figure 10a–d show the long-term mean value of surface CO concentration for 2001–2015 from WDCGG sites, and model simulations driven with a priori and a posteriori emissions. All simulations provide similar

results for long-term mean value. Figure 10e–g show the improvement due to a posteriori emissions, derived by $\text{abs}(\text{CO}_{\text{aposteriori}} - \text{CO}_{\text{WDCGG}}) - \text{abs}(\text{CO}_{\text{apriori}} - \text{CO}_{\text{WDCGG}})$. Figure 10f demonstrates that CO emissions constrained with MOPITT profile data improved the model simulation at about half of the sites in the Northern Hemisphere, whereas the a posteriori emissions constrained with MOPITT column data are worse (Fig. 10e). Evaluating modeled tracer concentrations using surface in situ measurements is more challenging than evaluating long-term trends. Important sources of uncertainty include the representation error (e.g., Chang et al., 2015; Kharol et al., 2015) and vertical mixing of boundary layer (e.g., Castellanos et al., 2011; Cuchiara et al., 2014).

As our a posteriori simulation, particularly using emissions constrained with MOPITT profile data, results in significant improvement in the long-term trend and moderate improvement in the mean value, we believe these a posteriori estimates provide a better description for the long-term variation of global CO emissions. A remaining question to

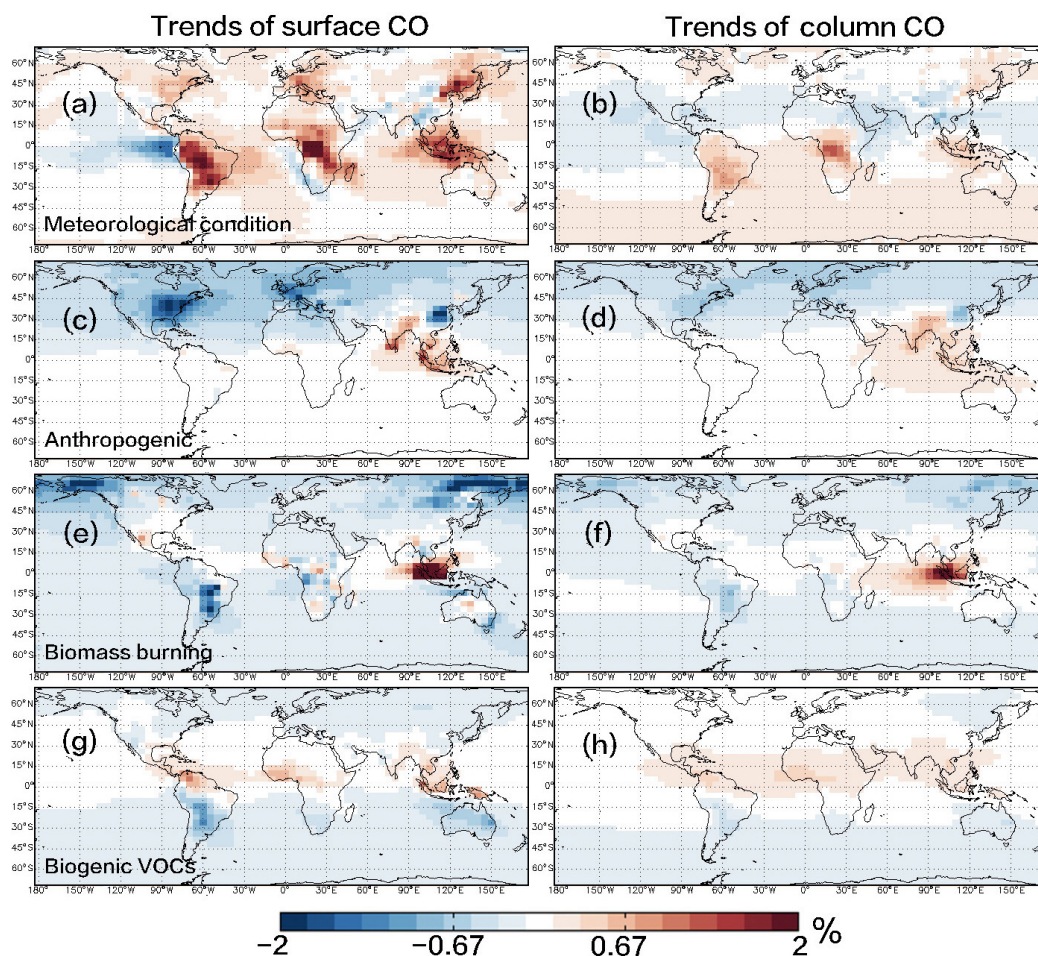


Figure 11. Long-term trend (annual) of modeled surface and column CO for 2001–2015 with (a–b) all emission sources fixed at the 2001 level. (c–d) Variable anthropogenic emissions; (e–f) variable biomass burning emissions; (g–h) variable biogenic VOCs emissions. The variable emissions are constrained with MOPITT profile data.

explore is how changes in meteorological conditions affect the long-term variation. By fixing CO emissions to 2001 levels, Fig. 11a–b show the long-term trend of modeled surface and column CO during 2001–2015, due only to changes in meteorological conditions. At the surface level (Fig. 11a), we found changes in meteorology result in a moderate positive trend in the Northern Hemisphere, particularly over northeast Asia, consistent with observation records from the TAP station, and significant positive trend in tropics, consistent with observation record from ASC station. On the other hand, the influence of meteorological conditions on column CO (Fig. 11b) is much weaker. The discrepancy between surface and column CO suggests a possible contribution from variable convective transport. It should be noted that our analysis for the contributions from meteorological conditions could be affected by the discrepancies among various versions of the meteorological fields (i.e., GEOS-4, GEOS-5 and GEOS-FP) and the lack of consistency in model physics of GEOS-5

(e.g., the transition from GEOS 5.1.0 to GEOS 5.2.0 in late 2008).

Figure 11c–h show the variation of global tropospheric CO due to changes in emissions. Yin et al. (2015) indicated that the negative trend of tropospheric CO in the Northern Hemisphere is driven by decreasing anthropogenic emissions from North America, Europe and China. Along with reductions in anthropogenic emissions (Fig. 11c, d), we found the decrease of biomass burning emissions from boreal North America and boreal Asia (Fig. 11e, f) to be an important factor for this negative trend. In contrast to the emission reduction from North America, Europe and China, we found increasing anthropogenic emissions from India and southeast Asia, which result in a pronounced positive trend of tropospheric CO, while Yin et al. (2015) obtain a negative trend for this region. This discrepancy requires further study, and we will need to test the relative importance of the primary differences in our methods, i.e., models and inversion approaches, climatological OH (this study) vs. assimilated surface measurements of

CH₄ and MCF to update OH (Yin et al., 2015), and the use of MOPITT profile vs. column CO retrievals (Yin et al., 2015, assimilate only column CO).

5 Summary

The objective of this work is to investigate the dominant reasons for the observed variation of global tropospheric CO over the past 15 years. We provide an update for this critical question and also an updated CO emission estimates for model studies. In particular, we use surface measurements of MCF to evaluate changes in the sinks of atmospheric CO and constrain the sources using MOPITT CO measurements to explain the observed decrease in CO concentrations. Our two-step approach for estimating global CO emissions mitigates the effects of model errors due to inaccuracies in representing transport and chemistry processes, as well as measurement bias error.

Using the same approach as Montzka et al. (2011), we assess the variation of tropospheric OH (the primary CO sink) in the period of 2001–2015 using MCF measurements from WDCGG stations. Our result demonstrates negligible variation of global tropospheric OH in the past 15 years, and consequently we suggest that the global sink of CO due to chemical loss through OH has not likely changed during this time period. We therefore expect the decreasing trend of tropospheric CO in the Northern Hemisphere (e.g., Warner et al., 2013; Worden et al., 2013a; Gratz et al., 2015) to be driven by decreasing CO sources. Total anthropogenic CO emissions from the US were 56.8 Tg in 2015, which is 35 % lower than emissions in 2001 (87.7 Tg). Total anthropogenic CO emissions from east China were 159.0 Tg in 2015, which is 7 % lower than 2001 emissions (170.4 Tg) and 23 % lower than 2004 emissions (205.6 Tg). This pronounced decrease of emissions from the US and China is an indication of progress for fuel efficiency and emission control regulations. Conversely, our results demonstrate that anthropogenic emissions from Europe decreased from 2001 to 2007 but remained almost unchanged during 2008–2015. We also found a significant increase of anthropogenic emissions for India and southeast Asia. The total anthropogenic CO emission from India and southeast Asia was 130.4 Tg in 2015, which is 34 % higher than that in 2001 (97.5 Tg). Assuming the same emission growth rate as 2011–2015, we expect that anthropogenic CO emissions from India and southeast Asia will be larger than Chinese emissions by 2020.

In a recent study, Yin et al. (2015) indicated that the decreasing tropospheric CO in the Northern Hemisphere is caused by the decrease of anthropogenic emissions from North America, Europe and China. We find that a decrease of biomass burning emissions from boreal North America and boreal Asia is also an important contributor for the negative trend. Globally, our analysis indicates a negative trend of biomass burning emissions in the past 15 years, except in

Indonesia due to the strong biomass burning event in 2015 associated with El Niño. Our results demonstrate a significant decrease of biomass burning emissions from South America, which could be associated with the reduction of deforestation in Brazil (Reddington et al., 2015) and the predominant change from El Niño to La Niña in our study period (Andela et al., 2014). For Africa, there is no obvious CO emission trend in the past 15 years, consistent with previous results (Chevallier et al., 2009; Tosca et al., 2015; Andela et al., 2014). Our results are inconclusive in characterizing the CO sources from oxidation of biogenic VOCs. More efforts are needed in the future to better understand the mechanism for tropical CO emissions.

Our analysis highlights the importance of space-based instruments for monitoring changes in global pollutant emissions. Our results demonstrate successful emission controls in the US and China over the past 15 years and suggest that emission controls in Europe may need re-evaluation. We also recommend more efforts in the future to better understand the regional and global effects of increasing pollutant emissions from India and southeast Asia.

Data availability. The MOPITT data are available at <ftp://15eil01.larc.nasa.gov/MOPITT/MOP02J.006>. The MCF and CO measurements from WDCGG are available at <http://ds.data.jma.go.jp/gmd/wdcgg/>. MOPITT data sets used in this study are publicly available at <http://reverb.echo.nasa.gov> and at <https://eosweb.larc.nasa.gov/datapool>.

The Supplement related to this article is available online at doi:10.5194/acp-17-4565-2017-supplement.

Competing interests. The authors declare that they have no conflict of interest.

Acknowledgements. We thank the World Data Centre for Greenhouse Gases (WDCGG) for providing their CO and MCF data. The National Center for Atmospheric Research (NCAR) is sponsored by the National Science Foundation. The NCAR MOPITT project is supported by the National Aeronautics and Space Administration (NASA) Earth Observing System (EOS) Program. The MOPITT team also acknowledges support from the Canadian Space Agency (CSA), the Natural Sciences and Engineering Research Council (NSERC) and Environment Canada, along with the contributions of COMDEV (the prime contractor) and ABB BOMEM.

Edited by: J. Kuttippurath

Reviewed by: two anonymous referees

References

- Andela, N. and van der Werf, G.: Recent trends in African fires driven by cropland expansion and El Niño to La Niña transition, *Nature Climate Change* 4, 791–795, doi:10.1038/nclimate2313, 2014.
- Arellano, A., Kasibhatla, P., Giglio, L., Werf, G., Randerson, J., and Collatz, G.: Time-dependent inversion estimates of global biomass-burning CO emissions using Measurement of Pollution in the Troposphere (MOPITT) measurements, *J. Geophys. Res.-Atmos.*, 111, D09303, doi:10.1029/2005JD006613, 2006.
- Bergamaschi, P., Frankenberg, C., Meirink, J., Krol, M., Dentener, F., Wagner, T., Platt, U., Kaplan, J., Körner, S., Heimann, M., Dlugokencky, E., and Goede, A.: Satellite cartography of atmospheric methane from SCIAMACHY on board ENVISAT: 2. Evaluation based on inverse model simulations, *J. Geophys. Res.-Atmos.*, 112, D02304, doi:10.1029/2006JD007268, 2007.
- Bergamaschi, P., Frankenberg, C., Meirink, J., Krol, M., Villani, M., Houweling, S., Dentener, F., Dlugokencky, E., Miller, J., Gatti, L., Engel, A., and Levin, I.: Inverse modeling of global and regional CH₄ emissions using SCIAMACHY satellite retrievals, *J. Geophys. Res.-Atmos.*, 114, D22301, doi:10.1029/2009JD012287, 2009.
- Bergamaschi, P., Houweling, S., Segers, A., Krol, M., Frankenberg, C., Scheepmaker, R., Dlugokencky, E., Wofsy, S., Kort, E., Sweeney, C., Schuck, T., Brenninkmeijer, C., Chen, H., Beck, V., and Gerbig, C.: Atmospheric CH₄ in the first decade of the 21st century: Inverse modeling analysis using SCIAMACHY satellite retrievals and NOAA surface measurements, *J. Geophys. Res.-Atmos.*, 118, 7350–7369, doi:10.1002/jgrd.50480, 2013.
- Bloom, A., Worden, J., Jiang, Z., Worden, H., Kurosu, T., Frankenberg, C., and Schimel, D.: Remote-sensing constraints on South America fire traits by Bayesian fusion of atmospheric and surface data, *Geophys. Res. Lett.*, 42, 1268–1274, doi:10.1002/2014GL02584, 2015.
- Bousquet, P., Hauglustaine, D. A., Peylin, P., Carouge, C., and Ciais, P.: Two decades of OH variability as inferred by an inversion of atmospheric transport and chemistry of methyl chloroform, *Atmos. Chem. Phys.*, 5, 2635–2656, doi:10.5194/acp-5-2635-2005, 2005.
- Bousserez, N., Henze, D., Perkins, A., Bowman, K., Lee, M., Liu, J., Deng, F., and Jones, D.: Improved analysis-error covariance matrix for high-dimensional variational inversions: application to source estimation using a 3D atmospheric transport model, *Q. J. Roy. Meteor. Soc.*, 141, 1906–1921, doi:10.1002/qj.2495, 2015.
- Bruhwyler, L., Dlugokencky, E., Masarie, K., Ishizawa, M., Andrews, A., Miller, J., Sweeney, C., Tans, P., and Worthy, D.: CarbonTracker-CH₄: an assimilation system for estimating emissions of atmospheric methane, *Atmos. Chem. Phys.*, 14, 8269–8293, doi:10.5194/acp-14-8269-2014, 2014.
- Castellanos, P., Marufu, L., Doddridge, B., Taubman, B., Schwab, J., Hains, J., Ehrman, S., and Dickerson, R.: Ozone, oxides of nitrogen, and carbon monoxide during pollution events over the eastern United States: An evaluation of emissions and vertical mixing, *J. Geophys. Res.-Atmos.*, 116, D16307, doi:10.1029/2010JD014540, 2011.
- Chang, K.-L., Guillas, S., and Fioletov, V. E.: Spatial mapping of ground-based observations of total ozone, *Atmos. Meas. Tech.*, 8, 4487–4505, doi:10.5194/amt-8-4487-2015, 2015.
- Chevallier, F., Fortems, A., Bousquet, P., Pison, I., Szopa, S., Devaux, M., and Hauglustaine, D. A.: African CO emissions between years 2000 and 2006 as estimated from MOPITT observations, *Biogeosciences*, 6, 103–111, doi:10.5194/bg-6-103-2009, 2009.
- Cuchiara, G. C., Li, X., Carvalho, J., and Rappenglück, B.: Inter-comparison of planetary boundary layer parameterization and its impacts on surface ozone concentration in the WRF/Chem model for a case study in Houston/Texas, *Atmos. Environ.*, 96, 175–185, doi:10.1016/j.atmosenv.2014.07.013, 2014.
- Deeter, M., Worden, H., Gille, J., Edwards, D., Mao, D., and Drummond, J.: MOPITT multispectral CO retrievals: Origins and effects of geophysical radiance errors, *J. Geophys. Res.-Atmos.*, 116, D15303, doi:10.1029/2011JD015703, 2011.
- Deeter, M. N., Martínez-Alonso, S., Edwards, D. P., Emmons, L. K., Gille, J. C., Worden, H. M., Sweeney, C., Pittman, J. V., Daube, B. C., and Wofsy, S. C.: The MOPITT Version 6 product: algorithm enhancements and validation, *Atmos. Meas. Tech.*, 7, 3623–3632, doi:10.5194/amt-7-3623-2014, 2014.
- Deng, F., Jones, D. B. A., Henze, D. K., Bousserez, N., Bowman, K. W., Fisher, J. B., Nassar, R., O'Dell, C., Wunch, D., Wennberg, P. O., Kort, E. A., Wofsy, S. C., Blumenstock, T., Deutscher, N. M., Griffith, D. W. T., Hase, F., Heikkinen, P., Sherlock, V., Strong, K., Sussmann, R., and Warneke, T.: Inferring regional sources and sinks of atmospheric CO₂ from GOSAT XCO₂ data, *Atmos. Chem. Phys.*, 14, 3703–3727, doi:10.5194/acp-14-3703-2014, 2014.
- Duncan, B., Lamsal, L., Thompson, A., Yoshida, Y., Lu, Z., Streets, D., Hurwitz, M., and Pickering, K.: A space-based, high-resolution view of notable changes in urban NO_x pollution around the world (2005–2014), *J. Geophys. Res.-Atmos.*, 121, 976–996, doi:10.1002/2015JD024121, 2016.
- Evans, M. J. and Jacob, D. J.: Impact of new laboratory studies of N₂O₅ hydrolysis on global model budgets of tropospheric nitrogen oxides, ozone, and OH, *Geophys. Res. Lett.*, 32, L09813, doi:10.1029/2005GL022469, 2005.
- Field, R., Werf, G., Fanin, T., Fetzer, E., Fuller, R., Jethva, H., Levy, R., Livesey, N., Luo, M., Torres, O., and Worden, H.: Indonesian fire activity and smoke pollution in 2015 show persistent non-linear sensitivity to El Niño-induced drought, *P. Natl. Acad. Sci. USA*, 113, 9204–9209, doi:10.1073/pnas.1524888113, 2016.
- Fortems-Cheiney, A., Chevallier, F., Pison, I., Bousquet, P., Szopa, S., Deeter, M., and Clerbaux, C.: Ten years of CO emissions as seen from Measurements of Pollution in the Troposphere (MOPITT), *J. Geophys. Res.-Atmos.*, 116, D05304, doi:10.1029/2010JD014416, 2011.
- Fortems-Cheiney, A., Chevallier, F., Pison, I., Bousquet, P., Saunio, M., Szopa, S., Cressot, C., Kurosu, T. P., Chance, K., and Fried, A.: The formaldehyde budget as seen by a global-scale multi-constraint and multi-species inversion system, *Atmos. Chem. Phys.*, 12, 6699–6721, doi:10.5194/acp-12-6699-2012, 2012.
- Gonzi, S., Feng, L., and Palmer, P.: Seasonal cycle of emissions of CO inferred from MOPITT profiles of CO: Sensitivity to pyroconvection and profile retrieval assumptions, *Geophys. Res. Lett.*, 38, L08813, doi:10.1029/2011GL046789, 2011.
- Gratz, L. E., Jaffe, D. A., and Hee, J. R.: Causes of increasing ozone and decreasing carbon monoxide in springtime at the Mt. Bachelor Observatory from 2004 to 2013, *Atmos. Environ.*, 109, 323–330, doi:10.1016/j.atmosenv.2014.05.076, 2015.

- Guenther, A., Karl, T., Harley, P., Wiedinmyer, C., Palmer, P. I., and Geron, C.: Estimates of global terrestrial isoprene emissions using MEGAN (Model of Emissions of Gases and Aerosols from Nature), *Atmos. Chem. Phys.*, 6, 3181–3210, doi:10.5194/acp-6-3181-2006, 2006.
- Heald, C., Jacob, D., Jones, D., Palmer, P., Logan, J., Streets, D., Sachse, G., Gille, J., Hoffman, R., and Nehr Korn, T.: Comparative inverse analysis of satellite (MOPITT) and aircraft (TRACE-P) observations to estimate Asian sources of carbon monoxide, *J. Geophys. Res.-Atmos.*, 109, D23306, doi:10.1029/2004JD005185, 2004.
- Henschel, S., Tertre, A., Atkinson, R., Querol, X., Pandolfi, M., Zeka, A., Haluza, D., Analitis, A., Katsouyanni, K., Bouland, C., Pascal, M., Medina, S., and Goodman, P.: Trends of nitrogen oxides in ambient air in nine European cities between 1999 and 2010, *Atmos. Environ.*, 117, 234–241, doi:10.1016/j.atmosenv.2015.07.013, 2015.
- Henze, D. K., Hakami, A., and Seinfeld, J. H.: Development of the adjoint of GEOS-Chem, *Atmos. Chem. Phys.*, 7, 2413–2433, doi:10.5194/acp-7-2413-2007, 2007.
- Hidy, G. M., Blanchard, C. L., Baumann, K., Edgerton, E., Tanenbaum, S., Shaw, S., Knipping, E., Tombach, I., Jansen, J., and Walters, J.: Chemical climatology of the southeastern United States, 1999–2013, *Atmos. Chem. Phys.*, 14, 11893–11914, doi:10.5194/acp-14-11893-2014, 2014.
- Hilboll, A., Richter, A., and Burrows, J. P.: Long-term changes of tropospheric NO₂ over megacities derived from multiple satellite instruments, *Atmos. Chem. Phys.*, 13, 4145–4169, doi:10.5194/acp-13-4145-2013, 2013.
- Hooghiemstra, P., Krol, M., Leeuwen, T., Werf, G., Novelli, P., Deeter, M., Aben, I., and Röckmann, T.: Interannual variability of carbon monoxide emission estimates over South America from 2006 to 2010, *J. Geophys. Res.-Atmos.*, 117, D15308, doi:10.1029/2012JD017758, 2012.
- Houweling, S., Krol, M., Bergamaschi, P., Frankenberg, C., Dlugokencky, E. J., Morino, I., Notholt, J., Sherlock, V., Wunch, D., Beck, V., Gerbig, C., Chen, H., Kort, E. A., Röckmann, T., and Aben, I.: A multi-year methane inversion using SCIAMACHY, accounting for systematic errors using TCCON measurements, *Atmos. Chem. Phys.*, 14, 3991–4012, doi:10.5194/acp-14-3991-2014, 2014.
- Huang, L., Fu, R., and Jiang, J. H.: Impacts of fire emissions and transport pathways on the interannual variation of CO in the tropical upper troposphere, *Atmos. Chem. Phys.*, 14, 4087–4099, doi:10.5194/acp-14-4087-2014, 2014.
- Inness, A., Benedetti, A., Flemming, J., Huijnen, V., Kaiser, J. W., Parrington, M., and Remy, S.: The ENSO signal in atmospheric composition fields: emission-driven versus dynamically induced changes, *Atmos. Chem. Phys.*, 15, 9083–9097, doi:10.5194/acp-15-9083-2015, 2015.
- Jiang, Z., Jones, D., Kopacz, M., Liu, J., Henze, D., and Heald, C.: Quantifying the impact of model errors on top-down estimates of carbon monoxide emissions using satellite observations, *J. Geophys. Res.-Atmos.*, 116, D15306, doi:10.1029/2010JD015282, 2011.
- Jiang, Z., Jones, D., Worden, H., Deeter, M., Henze, D., Worden, J., Bowman, K., Brenninkmeijer, C., and Schuck, T.: Impact of model errors in convective transport on CO source estimates inferred from MOPITT CO retrievals, *J. Geophys. Res.-Atmos.*, 118, 2073–2083, doi:10.1002/jgrd.50216, 2013.
- Jiang, Z., Jones, D. B. A., Worden, H. M., and Henze, D. K.: Sensitivity of top-down CO source estimates to the modeled vertical structure in atmospheric CO, *Atmos. Chem. Phys.*, 15, 1521–1537, doi:10.5194/acp-15-1521-2015, 2015a.
- Jiang, Z., Jones, D. B. A., Worden, J., Worden, H. M., Henze, D. K., and Wang, Y. X.: Regional data assimilation of multi-spectral MOPITT observations of CO over North America, *Atmos. Chem. Phys.*, 15, 6801–6814, doi:10.5194/acp-15-6801-2015, 2015b.
- Jiang, Z., Worden, J. R., Jones, D. B. A., Lin, J.-T., Verstraeten, W. W., and Henze, D. K.: Constraints on Asian ozone using Aura TES, OMI and Terra MOPITT, *Atmos. Chem. Phys.*, 15, 99–112, doi:10.5194/acp-15-99-2015, 2015c.
- Jones, D. B. A., Bowman, K. W., Logan, J. A., Heald, C. L., Liu, J., Luo, M., Worden, J., and Drummond, J.: The zonal structure of tropical O₃ and CO as observed by the Tropospheric Emission Spectrometer in November 2004 – Part 1: Inverse modeling of CO emissions, *Atmos. Chem. Phys.*, 9, 3547–3562, doi:10.5194/acp-9-3547-2009, 2009.
- Kharol, S. K., Martin, R. V., Philip, S., Boys, B., Lamsal, L. N., Jerrett, M., Brauer, M., Crouse, D. L., McLinden, C., and Burnett, R. T.: Assessment of the magnitude and recent trends in satellite-derived ground-level nitrogen dioxide over North America, *Atmos. Environ.*, 118, 236–245, doi:10.1016/j.atmosenv.2015.08.011, 2015.
- Kopacz, M., Jacob, D., Henze, D., Heald, C., Streets, D., and Zhang, Q.: Comparison of adjoint and analytical Bayesian inversion methods for constraining Asian sources of carbon monoxide using satellite (MOPITT) measurements of CO columns, *J. Geophys. Res.-Atmos.*, 114, D04305, doi:10.1029/2007JD009264, 2009.
- Kopacz, M., Jacob, D. J., Fisher, J. A., Logan, J. A., Zhang, L., Megretskaya, I. A., Yantosca, R. M., Singh, K., Henze, D. K., Burrows, J. P., Buchwitz, M., Khlystova, I., McMillan, W. W., Gille, J. C., Edwards, D. P., Eldering, A., Thouret, V., and Nedelec, P.: Global estimates of CO sources with high resolution by adjoint inversion of multiple satellite datasets (MOPITT, AIRS, SCIAMACHY, TES), *Atmos. Chem. Phys.*, 10, 855–876, doi:10.5194/acp-10-855-2010, 2010.
- Krol, M., vanLeeuwen, P. J., and Lelieveld, J.: Global OH trend inferred from methylchloroform measurements, *J. Geophys. Res.*, 103, 10697–10711, doi:10.1029/98JD00459, 1998.
- Kuhns, H., Green, M., and Etyemezian, V.: Big Bend Regional Aerosol and Visibility Observational (BRAVO) Study Emissions Inventory, Report prepared for BRAVO Steering Committee, Desert Research Institute, Las Vegas, Nevada, 2003.
- Kumar, A., Wu, S., Weise, M. F., Honrath, R., Owen, R. C., Helmig, D., Kramer, L., Val Martin, M., and Li, Q.: Free-troposphere ozone and carbon monoxide over the North Atlantic for 2001–2011, *Atmos. Chem. Phys.*, 13, 12537–12547, doi:10.5194/acp-13-12537-2013, 2013.
- Lelieveld, J., Dentener, F. J., Peters, W., and Krol, M. C.: On the role of hydroxyl radicals in the self-cleansing capacity of the troposphere, *Atmos. Chem. Phys.*, 4, 2337–2344, doi:10.5194/acp-4-2337-2004, 2004.
- Liu, F., Zhang, Q., Tong, D., Zheng, B., Li, M., Huo, H., and He, K. B.: High-resolution inventory of technologies, activities,

- and emissions of coal-fired power plants in China from 1990 to 2010, *Atmos. Chem. Phys.*, 15, 13299–13317, doi:10.5194/acp-15-13299-2015, 2015.
- Logan, J., Megretskaia, I., Nassar, R., Murray, L., Zhang, L., Bowman, K., Worden, H., and Luo, M.: Effects of the 2006 El Niño on tropospheric composition as revealed by data from the Tropospheric Emission Spectrometer (TES), *Geophys. Res. Lett.*, 35, L03816, doi:10.1029/2007GL031698, 2008.
- Meirink, J., Bergamaschi, P., Frankenberg, C., d'Amelio, M., Dlugokencky, E., Gatti, L., Houweling, S., Miller, J., Röckmann, T., Villani, M., and Krol, M.: Four-dimensional variational data assimilation for inverse modeling of atmospheric methane emissions: Analysis of SCIAMACHY observations, *J. Geophys. Res.-Atmos.*, 113, D17301, doi:10.1029/2007JD009740, 2008.
- Miyazaki, K., Eskes, H. J., and Sudo, K.: A tropospheric chemistry reanalysis for the years 2005–2012 based on an assimilation of OMI, MLS, TES, and MOPITT satellite data, *Atmos. Chem. Phys.*, 15, 8315–8348, doi:10.5194/acp-15-8315-2015, 2015.
- Montzka, S. A., Krol, M., Dlugokencky, E., Hall, B., Jöckel, P., and Lelieveld, J.: Small Interannual Variability of Global Atmospheric Hydroxyl, *Science*, 331, 67–69, doi:10.1126/science.1197640, 2011.
- Ohara, T., Akimoto, H., Kurokawa, J., Horii, N., Yamaji, K., Yan, X., and Hayasaka, T.: An Asian emission inventory of anthropogenic emission sources for the period 1980–2020, *Atmos. Chem. Phys.*, 7, 4419–4444, doi:10.5194/acp-7-4419-2007, 2007.
- Olivier, J. G. J. and Berdowski, J. J. M.: Global emissions sources and sinks, in: *The Climate System*, edited by: Berdowski, J., Guicherit, R., and Heij, B. J., A. A. Balkema Publishers/Swets & Zeitlinger Publishers, Lisse, the Netherlands, 33–78, 2001.
- Pfister, G., Hess, P., Emmons, L., Lamarque, J. -F., Wiedinmyer, C., Edwards, D., Pétron, G., Gille, J., and Sachse, G.: Quantifying CO emissions from the 2004 Alaskan wildfires using MOPITT CO data, *Geophys. Res. Lett.*, 32, L11809, doi:10.1029/2005GL022995, 2005.
- Prinn, R., Huang, J., Weiss, R., Cunnold, D., Fraser, P., Simmonds, P., McCulloch, A., Harth, C., Reimann, S., Salameh, P., O'Doherty, S., Wang, R., Porter, L., Miller, B., and Krummel, P.: Evidence for variability of atmospheric hydroxyl radicals over the past quarter century, *Geophys. Res. Lett.*, 32, L07809, doi:10.1029/2004GL022228, 2005.
- Reddington, C., Butt, E., Ridley, D., Artaxo, P., Morgan, W., Coe, H., and Spracklen, D.: Air quality and human health improvements from reductions in deforestation-related fire in Brazil, *Nat. Geosci.*, 8, 768–771, doi:10.1038/ngeo2535, 2015.
- Schneider, P., Lahoz, W. A., and van der A, R.: Recent satellite-based trends of tropospheric nitrogen dioxide over large urban agglomerations worldwide, *Atmos. Chem. Phys.*, 15, 1205–1220, doi:10.5194/acp-15-1205-2015, 2015.
- Spivakovsky, C. M., Logan, J. A., Montzka, S. A., Balkanski, Y. J., Foreman-Fowler, M., Jones, D. B. A., Horowitz, L. W., Fusco, A. C., Brenninkmeijer, C. A. M., Prather, M. J., Wofsy, S. C., and McElroy, M. B.: Three-dimensional climatological distribution of tropospheric OH Update and evaluation, *J. Geophys. Res.*, 105, 8931–8980, doi:10.1029/1999JD901006, 2000.
- Streets, D., Zhang, Q., Wang, L., He, K., Hao, J., Wu, Y., Tang, Y., and Carmichael, G.: Revisiting China's CO emissions after the Transport and Chemical Evolution over the Pacific (TRACE-P) mission: Synthesis of inventories, atmospheric modeling, and observations, *J. Geophys. Res.-Atmos.*, 111, D14306, doi:10.1029/2006JD007118, 2006.
- Strode, S. A., Worden, H. M., Damon, M., Douglass, A. R., Duncan, B. N., Emmons, L. K., Lamarque, J.-F., Manyin, M., Oman, L. D., Rodriguez, J. M., Strahan, S. E., and Tilmes, S.: Interpreting space-based trends in carbon monoxide with multiple models, *Atmos. Chem. Phys.*, 16, 7285–7294, doi:10.5194/acp-16-7285-2016, 2016.
- Stroppiana, D., Brivio, P. A., Grégoire, J.-M., Liousse, C., Guillaume, B., Granier, C., Mieville, A., Chin, M., and Pétron, G.: Comparison of global inventories of CO emissions from biomass burning derived from remotely sensed data, *Atmos. Chem. Phys.*, 10, 12173–12189, doi:10.5194/acp-10-12173-2010, 2010.
- Tohjima, Y., Kubo, M., Minejima, C., Mukai, H., Tanimoto, H., Ganshin, A., Maksyutov, S., Katsumata, K., Machida, T., and Kita, K.: Temporal changes in the emissions of CH₄ and CO from China estimated from CH₄/CO₂ and CO/CO₂ correlations observed at Hateruma Island, *Atmos. Chem. Phys.*, 14, 1663–1677, doi:10.5194/acp-14-1663-2014, 2014.
- Tosca, M., Diner, D., Garay, M., and Kalashnikova, O.: Human-caused fires limit convection in tropical Africa: First temporal observations and attribution, *Geophys. Res. Lett.*, 42, 6492–6501, doi:10.1002/2015GL065063, 2015.
- Turquety, S., Logan, J., Jacob, D., Hudman, R., Leung, F., Heald, C., Yantosca, R., Wu, S., Emmons, L., Edwards, D., and Sachse, G.: Inventory of boreal fire emissions for North America in 2004: Importance of peat burning and pyroconvective injection, *J. Geophys. Res.-Atmos.*, 112, D12S03, doi:10.1029/2006JD007281, 2007.
- Turner, A. J., Jacob, D. J., Wecht, K. J., Maasackers, J. D., Lundgren, E., Andrews, A. E., Biraud, S. C., Boesch, H., Bowman, K. W., Deutscher, N. M., Dubey, M. K., Griffith, D. W. T., Hase, F., Kuze, A., Notholt, J., Ohyama, H., Parker, R., Payne, V. H., Sussmann, R., Sweeney, C., Velasco, V. A., Warneke, T., Wennberg, P. O., and Wunch, D.: Estimating global and North American methane emissions with high spatial resolution using GOSAT satellite data, *Atmos. Chem. Phys.*, 15, 7049–7069, doi:10.5194/acp-15-7049-2015, 2015.
- van der Werf, G. R., Randerson, J. T., Giglio, L., Collatz, G. J., Kasibhatla, P. S., and Arellano Jr., A. F.: Interannual variability in global biomass burning emissions from 1997 to 2004, *Atmos. Chem. Phys.*, 6, 3423–3441, doi:10.5194/acp-6-3423-2006, 2006.
- van der Werf, G. R., Randerson, J. T., Giglio, L., Collatz, G. J., Mu, M., Kasibhatla, P. S., Morton, D. C., DeFries, R. S., Jin, Y., and van Leeuwen, T. T.: Global fire emissions and the contribution of deforestation, savanna, forest, agricultural, and peat fires (1997–2009), *Atmos. Chem. Phys.*, 10, 11707–11735, doi:10.5194/acp-10-11707-2010, 2010.
- van Leeuwen, T. T. and van der Werf, G. R.: Spatial and temporal variability in the ratio of trace gases emitted from biomass burning, *Atmos. Chem. Phys.*, 11, 3611–3629, doi:10.5194/acp-11-3611-2011, 2011.
- Vestreng, V. and Klein, H.: Emission data reported to UNECE/EMEP, Quality assurance and trend analysis and Presentation of WebDab, Norwegian Meteorological Institute, Oslo, Norway, MSC-W Status Report, 2002.

- Warner, J., Carminati, F., Wei, Z., Lahoz, W., and Attié, J.-L.: Tropospheric carbon monoxide variability from AIRS under clear and cloudy conditions, *Atmos. Chem. Phys.*, 13, 12469–12479, doi:10.5194/acp-13-12469-2013, 2013.
- Worden, H., Deeter, M., Edwards, D., Gille, J., Drummond, J., and Nédélec, P.: Observations of near-surface carbon monoxide from space using MOPITT multispectral retrievals, *J. Geophys. Res.-Atmos.*, 115, D18314, doi:10.1029/2010JD014242, 2010.
- Worden, H. M., Deeter, M. N., Frankenberg, C., George, M., Nichitiu, F., Worden, J., Aben, I., Bowman, K. W., Clerbaux, C., Coheur, P. F., de Laat, A. T. J., Detweiler, R., Drummond, J. R., Edwards, D. P., Gille, J. C., Hurtmans, D., Luo, M., Martínez-Alonso, S., Massie, S., Pfister, G., and Warner, J. X.: Decadal record of satellite carbon monoxide observations, *Atmos. Chem. Phys.*, 13, 837–850, doi:10.5194/acp-13-837-2013, 2013a.
- Worden, J., Wecht, K., Frankenberg, C., Alvarado, M., Bowman, K., Kort, E., Kulawik, S., Lee, M., Payne, V., and Worden, H.: CH₄ and CO distributions over tropical fires during October 2006 as observed by the Aura TES satellite instrument and modeled by GEOS-Chem, *Atmos. Chem. Phys.*, 13, 3679–3692, doi:10.5194/acp-13-3679-2013, 2013b.
- Xia, Y., Zhao, Y., and Nielsen, C.: Benefits of China's efforts in gaseous pollutant control indicated by the bottom-up emissions and satellite observations 2000–2014, *Atmos. Environ.*, 136, 43–53, doi:10.1016/j.atmosenv.2016.04.013, 2016.
- Yin, Y., Chevallier, F., Ciais, P., Broquet, G., Fortems-Cheiney, A., Pison, I., and Saunoy, M.: Decadal trends in global CO emissions as seen by MOPITT, *Atmos. Chem. Phys.*, 15, 13433–13451, doi:10.5194/acp-15-13433-2015, 2015.
- Yurganov, L. N., Duchatelet, P., Dzhola, A. V., Edwards, D. P., Hase, F., Kramer, I., Mahieu, E., Mellqvist, J., Notholt, J., Novelli, P. C., Rockmann, A., Scheel, H. E., Schneider, M., Schulz, A., Strandberg, A., Sussmann, R., Tanimoto, H., Velasco, V., Drummond, J. R., and Gille, J. C.: Increased Northern Hemispheric carbon monoxide burden in the troposphere in 2002 and 2003 detected from the ground and from space, *Atmos. Chem. Phys.*, 5, 563–573, doi:10.5194/acp-5-563-2005, 2005.
- Zhang, Q., Streets, D. G., Carmichael, G. R., He, K. B., Huo, H., Kannari, A., Klimont, Z., Park, I. S., Reddy, S., Fu, J. S., Chen, D., Duan, L., Lei, Y., Wang, L. T., and Yao, Z. L.: Asian emissions in 2006 for the NASA INTEX-B mission, *Atmos. Chem. Phys.*, 9, 5131–5153, doi:10.5194/acp-9-5131-2009, 2009.
- Zhang, L., Li, Q. B., Jin, J., Liu, H., Livesey, N., Jiang, J. H., Mao, Y., Chen, D., Luo, M., and Chen, Y.: Impacts of 2006 Indonesian fires and dynamics on tropical upper tropospheric carbon monoxide and ozone, *Atmos. Chem. Phys.*, 11, 10929–10946, doi:10.5194/acp-11-10929-2011, 2011.
- Zhao, Y., Nielsen, C., McElroy, M., Zhang, L., and Zhang, J.: CO emissions in China: Uncertainties and implications of improved energy efficiency and emission control, *Atmos. Environ.*, 49, 103–113, doi:10.1016/j.atmosenv.2011.12.015, 2012.